Pharmacologic ATF6 Activation Confers Global Protection in Widespread Disease Models by Reprograming Cellular Proteostasis

Erik A. Blackwood[1], Khalid Azizi, M.S. [1], Donna J. Thuerauf, M.S. [1], Ryan J. Paxman [2], Lars Plate [2,3], Jeffery W. Kelly [2,3], R. Luke Wiseman, Ph.D. [2] and Christopher C. Glembotski, Ph.D. [1]*

[1]San Diego State University Heart Institute and the Department of Biology, San Diego State University, San Diego, CA 92182
[2]Department of Chemistry,
The Scripps Research Institute, La Jolla CA, 92037
[3]Department of Molecular Medicine,
The Scripps Research Institute, La Jolla CA, 92037

Short Title: Pharmacological ATF6 Activation Mitigates Cardiac Pathology

*Corresponding Author: Christopher C. Glembotski, the SDSU Heart Institute and Department of Biology, San Diego State University, 5500 Campanile Drive, San Diego, CA 92182, USA. Tel.: (619) 594-2959; FAX: (619) 594-5676; E-mail: cglembotski@mail.sdsu.edu

Summary:

Pharmacologic activation of stress-responsive signaling pathways provides a promising approach for ameliorating imbalances in proteostasis associated with diverse diseases. However, this approach has not been employed *in vivo*. Here, using a mouse model of myocardial ischemia/reperfusion, we showed that selective pharmacologic activation of the ATF6 arm of the unfolded protein response (UPR) during reperfusion, a typical clinical intervention point after myocardial infarction, transcriptionally reprograms proteostasis, ameliorates damage and preserves heart function. These effects were lost upon cardiac myocyte-specific *Atf6* deletion in the heart, demonstrating the critical role played by ATF6 in mediating pharmacologically activated proteostasis-based protection of the heart. Pharmacological activation of ATF6 was also protective in renal and cerebral ischemia/reperfusion models, demonstrating its widespread utility. Thus, pharmacologic activation of ATF6 represents a first-in-class proteostasis-based therapeutic strategy for ameliorating ischemia/reperfusion damage, underscoring its unique translational potential for treating a wide range of pathologies caused by imbalanced proteostasis.

Protein homeostasis, or proteostasis is maintained by pathways that coordinate protein synthesis and folding with the degradation of misfolded, potentially toxic proteins[1,21,2]. ER proteostasis is particularly important, since nearly one-third of all proteins are made and folded in the ER, then transported to their final destinations as integral membrane or soluble secreted proteins[3]. Imbalances in proteostasis cause or exacerbate numerous pathologies, spawning interest in the exogenous manipulation of proteostasis as a therapeutic approach for such diseases[4]. ER proteostasis is regulated by the unfolded protein response (UPR), a stress-responsive signaling pathway comprising three sensors/effectors of ER protein misfolding; PERK (protein kinase R [PKR]-like ER kinase), IRE1 (inositol requiring enzyme 1), and ATF6 (activating transcription factor 6)[5]. Considerable evidence supports ATF6, a transcriptional regulator of ER proteostasis, as a viable therapeutic target for exogenous manipulation of proteostasis[6-11]; however, such an approach has not been examined *in vivo.* Accordingly, here, we determined whether treatment with a pharmacological activator of ATF6 would reprogram proteostasis and mitigate pathology in a mouse model of ischemic diseases, such as those that affect the heart.

Ischemic heart disease is the leading cause of human deaths worldwide[12]. These deaths are mainly due to acute myocardial infarction (AMI), where thrombotic coronary artery occlusion causes rapid, irreparable ischemic injury to the heart, increasing susceptibility to progressive cardiac degeneration and eventual heart failure[13-15]. The treatment of choice for AMI is primary percutaneous coronary intervention, or coronary angioplasty[16], which results in reperfusion. While reperfusion limits ischemic injury, the reperfusion itself injures the heart, in part by increasing reactive oxygen species (ROS). ROS contribute to AMI injury, also known as ischemia/reperfusion (I/R) injury, mainly by damaging proteins, which impairs proteostasis[17,18]. In fact, reperfusion accounts for up to 50% of the final damage from AMI[19]; however, there is no clinically available intervention that mitigates reperfusion injury at the time of coronary angioplasty, underscoring the importance of developing therapies that reduce ROS during reperfusion[19]. Using a mouse model of global ATF6 deletion, we recently showed that, in the heart, ATF6 is responsible for the expression of a broad spectrum of genes not traditionally identified to as regulated by ATF6, including many antioxidant genes that could improve proteostasis during I/R[10]. While this genetic approach identified the potential importance of ATF6 as a novel therapeutic target for pharmacological intervention in I/R injury models, there have been no reports addressing whether a single arm of the UPR can be pharmacologically activated and shown to beneficial in any animal model of pathology.

We recently identified a compound that we call **147** in a high-throughput cell-based reporter screen, where it was shown to selectively induce only the ATF6 arm of the UPR[20]. Here, we examined the effects of pharmacological activation of ATF6 with **147** in a mouse model of AMI. We found that intravenous administration of **147** concurrently with AMI robustly and selectively activated ATF6 and downstream genes of the ATF6 gene program and protected the heart

from I/R damage; however, this protection was lost upon the genetic deletion of ATF6. Moreover, **147** had no deleterious effects in the absence of pathology, or in other tissues that were unaffected by I/R, an indicator of its safety. Remarkably, we found that by activating ATF6, **147** protected other tissues, including the brain, kidney, and liver, when they were subjected to maneuvers that induced I/R damage and impaired proteostasis. This is the first *in vivo* characterization of any compound that selectively activates a single arm of the UPR, demonstrating that **147** has significant potential as a novel therapeutic approach for treating I/R damage in a wide range of tissues.

Results:

ATF6 in cardiac myocytes protects the heart from I/R injury:

Given their roles in contraction, the viability of cardiac myocytes is crucial for heart function, and cardiac myocyte death during I/R leads to impairment of this function[17]. Accordingly, we examined the effects of I/R on proteostasis in isolated cardiac myocytes and in the mouse heart, positing that I/R dysregulates proteostasis, leading to activation of all three arms of the UPR, and that the ATF6 arm induces genes that adaptively reprogram proteostasis, decrease myocyte death and provide cardioprotection from I/R damage **(Fig. 1a)**. Consistent with this hypothesis was our finding that I/R activated ATF6, as well as the IRE1 and PERK arms of the UPR in cultured cardiac myocytes **(Supplementary Fig. 1a-d)**. As a measure of ATF6 activation, we examined the expression of two known ATF6 target genes, glucose regulated protein 78 kDa (*Grp78*), a well-studied ER HSP70 chaperone, also known as BiP[21], which participates in ER protein folding, and catalase (*Cat*), a prominent member of a novel antioxidant gene program recently shown to be induced by ATF6[10]. In accordance with the increased activity of ATF6 in response to I/R, both *Grp78* and *Cat* were induced in cultured cardiac myocytes **(Supplementary Fig. 1a, e, f, g)**.

To examine the effects of deleting ATF6 specifically from cardiac myocytes, *in vivo*, we made an ATF6 conditional knockout mouse (ATF6 cKO) in which *Atf6* was selectively deleted in cardiac myocytes of $ATF6^{fl/fl}$ mice using AAV9-cTnT-CRE **(Supplementary Fig. 2a, b)**. ATF6 cKO and wild type (WT) mice, the latter of which retain ATF6, were subjected to 30 min of surgical coronary artery ligation, followed by 24 hours of reperfusion (I/R), which mimics the reperfusion injury in AMI patients that occurs acutely, a time during which the extent of reperfusion injury is progressive[22]. In this model, I/R causes cardiac myocyte death and irreparable damage in the infarct zone **(Fig. 1b, black)**, where blood flow has been completely occluded. However, cardiac myocytes adjacent to the infarct, in the border zone **(Fig. 1b, red)**, are exposed to sub-lethal I/R and mount protective stress responses, such as the UPR, while the remote region **(Fig. 1b, blue)** is relatively unaffected[13,23]. Thus, protective stress responses in border zone myocytes conserve their viability, thereby reducing the size of the infarct. WT mice exhibited a robust activation of ATF6 in response to I/R, as evidenced by induction of the ATF6 target genes, *Grp78* and *Cat* in the border zone of hearts subjected to acute I/R **(Fig. 1c, e)**; however, this induction was lost in ATF6 cKO mice **(Fig. 1d, f)**. In contrast, the IRE1 target gene, *Erdj4,* and PERK target gene, *Atf4*, were similarly induced by I/R in WT and ATF6 cKO mouse hearts **(Supplementary Fig. 2c, d)**. However, compared to WT, ATF6 cKO mice had increased infarct sizes and plasma cardiac troponin I (cTnI) **(Fig. 1h, i)**, canonical indicators of cardiac injury, and exhibited increased lipid peroxidation **(Supplementary Fig. 2e)**, a measure of ROS-mediated damage. *Grp78* and *Cat* were also increased in hearts from patients with ischemic heart disease **(Fig. 1g)**, supporting the relevance of the ATF6 adaptive arm of the UPR in human pathology and validating the phenotypes observed in this mouse model of AMI. Thus, while all three arms of the UPR were activated in the ischemic mouse

heart, cardiac specific deletion of *Atf6* significantly increased heart damage in response to I/R, demonstrating the importance of the ATF6 arm of the UPR in mitigating I/R injury in the heart.

In the days following AMI, the infarct continues to expand and remodels to become a fibrotic scar, so the detrimental effects of I/R on cardiac function and performance are often more pronounced a week after infarction[13]. Therefore, to examine the effect of *Atf6* deletion on cardiac function and performance, mice were analyzed 7d after AMI. ATF6 cKO mice exhibited significantly reduced fractional shortening compared to WT, despite being aphenotypic at baseline **(Supplementary Fig. 2f; Supplementary Table 1)**. ATF6 cKO mice also exhibited exaggerated pathological cardiac hypertrophy and plasma cTnI **(Supplementary Fig. 2g-h)**. Notably, the levels of *Grp78* and *Cat* were lower in ATF6 cKO than WT mice at 7 days **(Supplementary Fig. 2i-j)**. When we examined gene expression at 1 and 7d after MI we found that induction of *Atf6* and its target genes remained increased through 7d post MI, although the level of induction was reduced compared to 1d post MI **(Supplementary Fig. 2k)**, indicating that the adaptive effects of ATF6-induced genes are likely exerted throughout at least the first week following MI.

Cardiac hemodynamics were also assessed in an *ex vivo* isolated perfused heart model that enables the precise measurement of the strength of cardiac pump function, i.e., left ventricular developed pressure (LVDP), with each contraction in response to I/R injury[10]. ATF6 cKO mouse hearts exhibited significantly lower recovery of LVDP and larger infarcts than WT hearts **(Fig. 1j, k)**. Collectively, these results show that ATF6 in cardiac myocytes protects from myocardial I/R injury.

Interestingly, I/R activated ATF6 less than tunicamycin, which is a strong, chemical inducer of ER protein misfolding and UPR activation **(Supplementary Fig. 1a)**. Importantly, this result suggests that during I/R there is a reserve of inactive ATF6 remaining that could still be activated. Accordingly, we hypothesize that selective pharmacologic activation of ATF6 could supplement the modest ATF6 activation achieved by I/R to enhance cardioprotection.

147 activates ATF6 and induces ATF6-target genes in cardiac myocytes:

The compound **147** was previously shown to specifically activate ATF6 in HEK293 cells through a canonical mechanism involving translocation of ATF6 from the ER to the Golgi, where it is cleaved by S1 and S2 proteases to release the active ATF6 transcription factor[20] **(Fig. 2a)**. The translocation of ATF6 out of the ER during protein misfolding is known to require a reduction of the inter- and intramolecular disulfide bonds in ATF6; however, neither the effects of **147** on ATF6, nor its mechanism of action have been studied in cardiac myocytes. Here, in cultured cardiac myocytes, a control compound that closely resembles **147** **(Fig. 2b)**, but does not activate ATF6, did not affect the disulfide bond status of ATF6, while **147** reduced intramolecular disulfide bonds in ATF6 **(Fig. 2c, lanes 7-10)**. Moreover, while the control compound did not activate any of the UPR pathways, **147** activated ATF6, but not PERK or IRE1 **(Supplementary Fig. 3a-**

d). Thus**,** in cardiac myocytes, **147** induced the canonical reduction of disulfide bonds in ATF6, which is associated with ATF6 translocation to the Golgi. Coordinate with the generation of the active, nuclear form of ATF6 in the Golgi was our finding that **147** increased the nuclear translocation of ATF6 in cardiac myocytes **(Fig. 2d)** and increased the specific cleavage/activation of ATF6 **(Supplementary Fig. 3a, b, g)**. Mechanistically, **147** increased the association of ATF6 with known ATF6 binding sites in the *Grp78* and *Cat* promoters **(Fig. 2e)**, and **147** increased protein levels of GRP78 and CAT **(Supplementary Fig. 3a, e, f)**. Intravenous administration of **147** activated ATF6 and increased *Grp78* and *Cat* expression in WT mouse hearts; however, this effect was completely absent in ATF6 cKO mice **(Fig. 2g-j; Supplementary Fig. 3h).** As a testament to the ability of **147** to activate only the ATF6 arm of the UPR was our finding that **147** had no effect on the expression levels of the IRE1 or PERK targets, *Erdj4* or *Atf4* in either WT or ATF6 cKO mouse hearts **(Supplementary Fig. 3i, j)**. Thus, **147** selectively activates the ATF6 arm of the UPR in the heart, *in vivo*, as it does in cultured cardiac myocytes.

147 improves ER proteostasis and decreases oxidative stress:

Mechanistically, we examined whether **147** could replicate the breadth of adaptive effects of ATF6 on ER proteostasis, such as increasing ER associated protein degradation (ERAD), which removes potentially toxic terminally misfolded proteins, increasing folding and subsequent secretion of proteins made in the ER, and enhancing protection against ER protein misfolding. Here, **147** increased ERAD, as measured by the rate of degradation of ectopically expressed TCRα^{24} **(Fig. 3a, b)**, increased the folding and secretion of protein from the ER pathway **(Fig. 3c)**, and protected cells from death in response to ER protein misfolding induced by tunicamycin **(Fig. 3d)**; importantly, all of these effects were lost upon knockdown of *Atf6*. Next we explored whether **147** could replicate the adaptive effects of ATF6 against oxidative stress, *in vitro*. **147** significantly improved survival of cardiac myocytes subjected to I/R **(Fig. 3e)** and decreased ROS-mediated damage **(Fig. 3f)**. Importantly, these effects of **147** were, again, lost upon knockdown of *Atf6*. Thus, **147** replicated a broad spectrum of the adaptive effects of ATF6 on proteostasis and oxidative stress. Moreover, all of these effects required endogenous ATF6, demonstrating the ATF6-dependent mechanism of action of **147**.

147 administered in vivo protects isolated cardiac myocytes and isolated-perfused hearts:

In an initial experiment to determine whether **147** retained its ability to protect myocytes *in vivo*, mice were treated for 24h with either the negative control compound or **147**, after which cardiac myocytes were isolated and subjected to I/R in culture. Compared to the negative control, myocytes from **147**-treated WT mice exhibited increased viability when subjected to I/R *in vitro* **(Fig. 3g, left)**; however, this benefit was absent in myocytes prepared from ATF6 cKO mice **(Fig. 3g, right)**. This demonstrated that when administered *in vivo*, **147** retained

its ability to protect cardiac myocytes from I/R damage in culture, and this protection was mediated through endogenous ATF6. To determine whether the protection seen in isolated cardiac myocytes had any effect in the intact heart, hearts from WT and ATF6 cKO mice that had been treated for 24h with **147** were examined in the *ex vivo* I/R model. Compared to control, hearts from **147-**treated WT mice had greater LVDP recovery and smaller infarct sizes **(Fig. 3h, blue vs red; 3i, left)**. Notably, **147** exhibited neither of these beneficial effects in hearts from ATF6 cKO mice **(Fig. 3h, gray and black; 3i, right)**. Thus, when administered to mice, **147** protected cardiac myocytes, and decreased I/R injury of the heart, while preserving cardiac function. Furthermore, all of these beneficial effects of **147** were dependent upon endogenous ATF6 in cardiac myocytes.

147 induces ATF6 target genes in the heart:

Next, the effects of **147** on ATF6 target gene induction in the hearts of mice that were not subjected to I/R were examined using several dosing protocols spanning 7 days **(Fig. 4a)**. Mice were injected with the negative control compound or **147** either twice, at days 0 and 4 (Trials 1 and 2, respectively), or **147** was injected only once, at day 0 (Trial 3). Compared to Trial 1, Trial 2 but not Trial 3 resulted in increased the expression of the ATF6-regulated genes *Grp78* and *Cat* **(Fig. 4b, c, e)** but not the IRE1-regulated *Erdj4* or the PERK-regulated *Atf4* **(Supplementary Fig. 4a, b).** These results indicated that that **147**-mediated induction of ATF6-target genes is transient, as gene induction was increased 3d after administration, but returned back to baseline 7d after administration. The transient nature of gene induction was supported by the relatively rapid clearance of **147** from plasma **(Fig. 4f)**.

Interestingly, Trial 2 significantly enhanced cardiac performance **(Fig. 4d; Trial 1 vs 2; Supplementary Table 2)**, which could be partly due to **147**-dependent increases in *Atp2a2* expression **(Supplementary Fig. 4c)**. *Atp2a2* encodes SERCA2a, an adaptive SR/ER-localized calcium ATPase previously shown to be ATF6-inducible in the heart[25] and to improve contractility in heart failure patients[26]. None of the **147** dosing protocols resulted in cardiodoxicity, as evidenced by no increased plasma cTnI **(Supplementary Fig. 4e)** or cardiac pathology-associated genes, such as *Nppa*, *Nppb*, *Col1a1* or *Myh7* **(Supplementary Fig. 4h)**. Furthermore, no apparent deficits were observed in any of the trials upon inspection of the liver or kidneys when steatosis and glomerular filtration rate were assessed by hepatic triglyceride accumulation and creatinine clearance, respecitvely **(Supplementary Fig. 4f, g)**. Finally, a time course of gene induction showed that *Atf6* and its target genes were induced at the earliest time point examined, i.e. 8h, reaching a maximum 24h after administration and falling back to baseline values by 7d after administration **(Supplementary Fig. 4i)**. These results indicate a time course of gene induction that is consistent with the time course of the protective effects of **147**.

147 protects the heart from I/R injury in vivo:

Next, the effects of **147** were examined in an *in vivo* model of I/R damage in the heart 7d after reperfusion **(Fig. 5a)**. In Trials 4 and 5, the negative control compound or **147**, respectively, were administered 24h prior to AMI, with a second dose at reperfusion and a third dose 4 days later. In Trial 6, **147** was administered at reperfusion and again 4 days later. In Trial 7, **147** was administered only one time at reperfusion. Given the transient nature of **147**, we designed our multiple-dose strategy so that it mimics a therapeutic approach used for treating AMI patients as soon as possible after the infarction, to mitigate the initial reperfusion damage to the heart, as well as days later to ameliorate the detrimental effects of continued expansion of infarct damage and cardiac remodeling in the infarct and infarct border zones on heart pump function. Strikingly, cardiac performance was preserved to similar extents in all trials of **147 (Fig. 5b)**, as was the ability of **147** to reduce cardiac hypertrophy, which is a pathological response to I/R in this model **(Fig. 5c)**. **147** decreased plasma cTnI in all trials, though somewhat less so in Trials 6 and 7 **(Fig. 5d)**. Importantly, **147** preserved diastolic cardiac function and left ventricular volumes in all of the trials **(Fig. 5e-g; Supplementary Table 3)**, showing that **147** impeded the progression toward heart failure. In Trials 5 and 6 the beneficial structural and functional effects were accompanied by increased expression of the ATF6-regulated genes, *Grp78* and *Cat* **(Fig. 5h, i)** but not *Erdj4* and *Atf4* **(Supplementary Fig. 5a-c)**. However, in Trial 7, expression of *Grp78* and *Cat* were comparable to control treated animals, as expected, given the transient nature of **147**-mediated gene induction seen in a previous experiment **(see Fig. 3)**. Moreover, as expected, I/R induced cardiac pathology genes **(Supplementary Fig. 5d, Sham vs Trial 4)**; however, these effects were blunted by **147 (Supplementary Fig. 5d, Trials 5-7)**. In addition, decreased levels of pro-apoptotic cleaved caspase-3 were seen in Trials 5-7 **(Supplementary Fig. 5e)**, indicating that **147** protected against I/R-induced myocyte apoptosis. Thus, pharmacologic ATF6 activation at reperfusion ameliorated pathologic cardiac dysfunction in response to I/R injury.

147 is beneficial in a wide range of proteostasis-mediated disease models, in vivo:

Next, we examined the effects of **147** following 24h of administration, an important time at which AMI patients are often treated by coronary angioplasty. Additionally, since ATF6 is expressed in all cells, we posited that it might be effective in tissues in addition to the heart. Accordingly, in addition to the heart, we determined the effects of **147** in the liver, kidney and brain. **147** activated ATF6 target genes in all four of the tissues, as evidenced by significant increases in of *Grp78* and *Cat* **(Fig. 6a, b)**, although the magnitude of the responses varied somewhat between tissues. The functionality of **147**-mediated activation of ATF6 in the liver was evident in that it significantly reduced ER protein misfolding, measured by XBP1 splicing, in mice that had been injected with tunicamycin; this beneficial effect was lost upon genetic deletion of ATF6 **(Fig. 6c)**. Additional evidence of the functionality of **147** in the liver was evident in its ability to reduce

hepatic triglycerides, a hallmark of hepatic steatosis, which demonstrates improved ER proteostasis in the liver **(Fig. 6d, blue)**; this beneficial effect of **147** was also lost upon deletion of ATF6 **(Fig. 6d, black)**.

Next, to examine the functional effects of **147** in the various tissues, the control compound or **147** were administered, as shown in **Figure 6e**, and the effects were examined on tissue damage in the heart via the acute I/R model, the kidney via transient unilateral renal portal system occlusion, and in the brain via transient unilateral middle cerebral artery occlusion. Throughout the studies, the surgeon and the data analyst were blinded to the animal assignments, which were predetermined by a separate investigator. Remarkably, even when administered only at the time of reperfusion, **147** significantly decreased infarct sizes in all three tissues when measured 24h after I/R **(Fig. 6f-h; Supplementary Fig. 6a)**. Moreover, **147** decreased plasma cTnI and creatinine, which are biomarkers of cardiac and kidney damage, respectively, and it improved behavioral indicators of post-ischemic neurological deficit **(Fig. 6i-k)**. As expected, since 24h after reperfusion is too short for structural remodeling there was no observable functional deficit on cardiac performance, chamber size, or pathological hypertrophy, as monitored by echocardiography **(Supplementary Table 4)**. As further proof of concept, this experiment was replicated in female mice and, again, both Trials 9 and 10 conferred protection as evidenced by reduced infarct sizes and plasma cTnI **(Supplementary Fig. 6b, c)**. Importantly, these beneficial effects of **147** in response to myocardial acute I/R were not seen in ATF6 cKO mice, further emphasizing that **147**-mediated protection of the heart required ATF6 activation **(Supplementary Fig. 6d, e)**. Interestingly, the beneficial effects of **147** were also seen in a different AMI model induced by acute administration of the β-adrenergic receptor agonist, isoproterenol, which is known to cause widespread oxidative damage and cardiac myocyte death in mice at this dose **(Supplementary Fig. 6f-h)**.

Thus, when administered at the time of injury, **147** was able to protect a wide range of tissues from I/R damage, emphasizing the broad spectrum of potential applications for this compound as a transcriptional regulator of the ATF6 arm of the UPR and subsequent reprogramming of proteostasis, *in vivo.*

Discussion:

After an AMI, upon reconstituting blood flow reperfusion damage begins almost immediately and continues for at least 3 days[27]. The initial reperfusion damage is thought to be due ROS generation by mitochondria in the myocardium, while the longer term damage may be due to multiple mechanisms, including continued ROS generation by the infiltration of inflammatory cells into the infarct zone[13,28]. Therefore, an effective therapy for AMI should function over a timeframe spanning at least 3 days. While a number of potential therapies that act acutely to minimize reperfusion damage have been tested, many of them have failed to move through the drug development process and there is still no clinically available intervention[15]. When we began the current study we posited that this might be because most of the previous therapeutics function only during the initial stages of reperfusion, losing efficacy in the ensuing days. Furthermore, many of the initial trials performed in small animals have not tested therapies at times that accurately mimic typical clinical interventions (i.e. during coronary angioplasty) and have not adhered to the FDA's Good Laboratory Practices (GLP). Accordingly, in addition to addressing these points in the design of our animal trials here, we examined the therapeutic function after both 1 and 7d of reperfusion. We also set out to develop a therapeutic approach that would exert beneficial effects through multiple mechanisms in various cellular locations, which we felt would broaden the potential utility to include different tissues and widen the scope to multiple proteostasis-based pathologies. In this regard, we focused on ATF6, since it adaptively reprograms ER proteostasis by inducing a wide range of protective response genes that encode proteins, such as catalase and grp78, which act to mitigate ROS-induced damage, as well as emending ROS-independent proteostasis pathways, respectively **(Supplementary Fig. 7)**. Using this strategy, we found that selective pharmacologic activation of only the ATF6 arm of the UPR with **147** in mice acted within 1d to reduce reperfusion damage in the heart and acted after 7d to preserve cardiac function. This timing of these beneficial effects is consistent with the timing of adaptive ATF6-target gene induction and the reperfusion damage that takes place over this same time frame. In addition to demonstrating its efficacy in the ischemic heart, we found that **147** protected the liver in a mouse model of dysregulated hepatic proteostasis, and it protected the kidneys and brain in models of renal and cerebral I/R damage. These findings, together with a recent report showing that **147** enhances the differentiation of human embryonic stem cells[29], support the broad therapeutic potential of pharmacologic activation of ATF6 for treating a wide range of proteostasis-based pathologies in various tissues.

In terms of its suitability as a pharmacologic agent, **147** exhibits many desirable properties. For example, **147** is highly specific, serving as the first example of a compound that selectively activates only one arm of the UPR, ATF6, which is well known for exerting mainly beneficial effects in many different cell types. **147** is highly efficacious *in vivo*, functioning at a dose similar to many other cardiovascular drugs and has the capacity to cross the blood brain barrier. Moreover, **147** does not exhibit any apparent toxicity or deleterious off-target effects *in vivo*. Both the efficacy and tolerance of **147** can be attributed in large

part to the high-stringency, cell-based transcriptional profiling that was done in the initial screening to ensure that **147** specifically activates only the ATF6 arm of the UPR, instead of global UPR activation[20]. The relatively transient activation of ATF6 by **147** *in vivo* is also potentially advantageous, since many stress-signaling pathways, including the UPR, can be beneficial initially, but damaging upon chronic activation[30]. Since I/R only partially activates ATF6, the remaining inactive ATF6 provides a therapeutic reserve for **147** to activate, allowing it to boost adaptive ATF6 signaling pathways in multiple tissues, *in vivo.* Remarkably, we found that **147** exerted beneficial effects in the hearts of mice that were not subjected to any injury maneuvers, underscoring the safety, and perhaps even benefits of the compound in healthy tissues. Thus, while future pharmacokinetic and toxicology studies will address further details of **147** action, it is clear from the results presented here that **147** is easily administered, well tolerated, acts quickly, boosts an endogenous adaptive transcriptional stress signaling pathway, and has no apparent off-target or untoward effects, all of which are attributes of an excellent candidate for therapeutic development.

Impaired proteostasis contributes to numerous pathologies and even impacts aging[31]. Thus, global improvement of proteome quality through pharmacologic activation of defined transcriptional regulators of proteostasis should ameliorate a broad range of proteostasis-based diseases. Recent findings showing that the sphere of influence of the UPR, in particular, the ATF6 arm of the UPR, extends well beyond the ER to reprogram proteostasis in many cellular locations[10], support the potential broad spectrum of impact of pharmacologic compounds, like **147**. The results presented here provide proof-of-principle that this type of pharmacologic correction can be achieved with well-characterized compounds, such as **147** that selectively activate a specific protective aspect of UPR signaling.

Acknowledgements: The authors wish to thank Dr. Gokhan S. Hotamisligil (Harvard T.H. Chan School of Public Health, Boston, MA) who generated and kindly provided the ATF6a fl/fl mice, Dr. Randal Kaufman (Sanford Burham Prebys Medical Discovery Institute, La Jolla, CA), who generated the global ATF6 knockout mice, and Dr. Oliver Muller (University of Kiel, Arnold-Heller-Str.3, Kiel, Germany), for providing us with the cTNT-Cre plasmid that was used to prepare AAV9. Human heart tissue was obtained from Dr. Kenneth B. Margulies (Heart Failure and Transplantation, Translational Research Center, Perelman School of Medicine, University of Pennsylvania, Philadelphia, PA). This work was supported by grants from the National Institutes of Health to C.C.G. (R01 HL75573, R01 HL104535, and P01 HL085577), J.W.K. ( ), R.L.W. (R01 DK102635, R01 DK107604, R01 NS092829, UL1TR001114), a fellowship to Lars Plate from the Leukemia and Lymphoma Society, and grants and fellowships to E.A.B. from the American Heart Association (17PRE33670796), Rees-Stealy Research Foundation and SDSU Heart Institute, the Inamori Foundation, and the ARCS Foundation, Inc., San Diego Chapter.

Author Contributions: EAB and CCG conceived of and designed the experiments with consultation and advice from JWK, LP and RLW. EAB did most of the experiments and a majority of the data analysis, DJT generated all of the AAV reagents and did some data analysis, KMA did some of the initial mouse I/R experiments and some data analysis; RJP synthesized the control compound and compound 147; EAB, CCG, RLW and JWK wrote the manuscript.

Competing Financial Interests:

None.

Fig. 1 –ATF6 in cardiac myocytes protects the heart from I/R injury.

a, Activation of the unfolded protein response (UPR) by ischemia/reperfusion (I/R) in the heart. **b,** Post-AMI cross section of the left ventricle of a mouse heart after I/R and TTC staining to identify the infarct region (black), border zone (red) and remote region (blue). **c, d,** Immunohistochemical (IHC) staining of GRP78 or CAT (cyan), tropomyosin (red), and nuclei (TOPRO-3) in the border zone of wild-type (WT) (**c**) or ATF6 cKO (**d**) hearts subjected to either sham or I/R surgery with 24h of reperfusion. Tissue sections are representative images from one mouse per condition. **e-g,** Quantitative real-time PCR (qPCR) for *Grp78* or *Cat* in sham or border zone of post-I/R hearts in WT (n=6) (**e**), ATF6 cKO (n=6) (**f**), or in ventricular explants from control (n=10) or ischemic heart failure (n=10) patients (**g**). **h,i,** Infarct sizes (**h**) and plasma cardiac troponin I (cTnI) (**i**) in WT (n=3) and ATF6 cKO (n=4) mice post-I/R. **j,k,** Left ventricular developed pressure (LVDP) (**j**) and relative infarct sizes (**k**) post-*ex vivo* I/R (n=3). Data are represented as mean ± s.e.m. **P*≤0.05, ***P*≤0.01, ****P*≤0.001.

Fig. 2 –147 selectively activates ATF6 in the heart.

a, Diagram of hypothetical mechanism of ATF6 activation by **147**. **b,** Chemical structure of synthetic control compound and compound **147**. **c,** Immunoblot of ATF6 and GAPDH in NRVM 24-hours after treatment with compound 147 or TM in fully-reducing condition (lanes 1-6) or non-reducing conditions (lanes 7-12). Shift exhibited in Atf6 in TM-treated cells in full-reducing conditions is typical of de-glycosylated ATF6. **d,** Immunocytofluorescence (ICF) of ATF6 (green), alpha-actinin (red) and nuclei (TOPRO-3) in NRVM 24-hours after treatment with compound **147**. **e,** Chromatin immunoprecipitation (ChIP-qPCR) of known ATF6 target promoter binding elements (ERSE) for Grp78 (*hspa5*), *cat*, and negative control targets Heme oxygenase 1 (*ho-1*) and *gapdh* NRVM infected with AdV encoding Flag-ATF6 (1-670) 24-hours after treatment with compound **147**(n=3). **f,** ICF of GRP78 and CAT (green), alpha-actinin (red) and nuclei (TOPRO-3) in AMVM 24-hours after treatment with compound **147**. **g, h,** qPCR for *Grp78* (n=6) or *Cat* (n=3) in LV of WT (**g**) or ATF6 cKO (**h**) hearts 24-hours post-treatment with control or **147**. **i,j,** IHC staining of GRP78 or CAT (cyan), tropomyosin (red), and nuclei (TOPRO-3) in left ventricle (LV) of WT (**i**) or ATF6 cKO (**j**) hearts 24-hours post-treatment with control or **147**. Tissue sections are representative images from one mouse per condition. Data are represented as mean ± s.e.m. **P*≤0.05, ***P*≤0.01, ****P*≤0.001.

Fig. 3 –147 improves proteostasis and decreases oxidative stress in an ATF6-dependent manner.

a, b, NRVM were infected with AdV-HA-T-cell antigen receptor alpha-chain (TCRα; an ER-transmembrane protein that is chronically misfolded and degraded by ERAD), treated with siCon or siAtf6 and either control or **147** for 24-hours prior to cyclohexamide for 0, 0.5 or 1h. Densitometry of the HA-TCRα

immunoblots at the respective times (**a**) and ERAD at the 0.5-hour time point (**b**) are shown (n=2). **c,** Secretory proteostasis assayed in NRVM when transfected with *Gaussia* luciferase and treated with siCon or siAtf6, and either control or **147** for 24-hours. Medium was collected and luciferase activity was measured (n=3). **d,** NRVM were transfected with siCon or siAtf6, then treated with or without TM, control or **147** for 24h, after which viability was determined (n=4). **e, f,** NRVM were transfected with siCon or siAtf6, treated with or without control or **147** for 24h, then I/R, after which viability (**e**) and MDA (**f**) were measured. **g,** Viability of I/R-treated cultured adult cardiomyocytes isolated from WT (n=3) or ATF6 cKO (n=3) mice 24-hours post-treatment with control or **147**. **h,i,** LVDP (**h**) and relative infarct sizes (**i**) of WT or ATF6 cKO mice treated 24h with control or **147** then *ex vivo* I/R. Data are represented as mean ± s.e.m. ***P*≤0.01, ****P*≤0.001.

Fig. 4 –147 gene induction timecourse, *in vivo*.

a, Experimental design testing the effects of **147** in WT untreated mice. Red bars depict the bolus administration of the control compound, while blue bars depict the bolus administration of **147**. **b, c,** qPCR for *Grp78* (**b**) or *Cat* (**c**) in LV of mice from indicated trials (n=3). **d,** Percent increase in fractional shortening. Detailed analyses of echocardiography parameters are in Extended Data Table 2 (n=5). **e,** IHC staining of GRP78 or CAT (cyan), tropomyosin (red), and nuclei (TOPRO-3) in LV of mice from respective trials. Tissue sections are representative images from one mouse per condition. **f,** 147 plasma concentration-time curve in mice receiving 2 mg/kg via venous injection. Blood was collected at baseline and 5-min, 15-min, 30-min, 1-hour, 2-hours, and 4-hours post injection (n=4 mice per timepoint). Data are represented as mean ± s.e.m. **P*≤0.05, ***P*≤0.01.

Fig. 5 –147 improves cardiac performance 7d post-AMI.

a, Experimental design for testing the effects of **147** in the hearts of mice subjected to 30 min of myocardial infarction, then examined 7d after the initiation of reperfusion. Red bars depict the bolus administration of the control compound, while blue bars depict the bolus administration of **147**. **b, f, g,** Echocardiographic parameters of fractional shortening (**b**), LV end diastolic volume (LVEDV) (**f**) and LV end systolic volume (LVESV) (**g**) (n=5). Detailed analyses of echocardiography parameters are in Extended Data Table 3. **c,** Ratio of heart weight to body weight (n=5). **d,** Plasma cTnI (n=5). **e,** Diastolic function as determined by pulse wave Doppler (PW) technique to analyze E and A waves (n=5). **h, i,** qPCR for *Grp78* (**h**) or *Cat* (**i**) in LV of mice from indicated trials at culmination of study (n=3). Data are represented as mean ± s.e.m. **P*≤0.05, ***P*≤0.01, ****P*≤0.001.

Fig. 6 –147 exerts widespread protection in multiple organ systems.

a, b, qPCR for *Grp78* (**a**) or *Cat* (**b**) in left ventricular, liver, kidney, and brain extracts from WT mice 24-hours post-treatment with control or **147** (n=3). **c,**

Ratio of transcript levels of *Xbp1s* to *Xbp1* as determined by qPCR in liver extracts from WT or ATF6 KO mice 24-hours post-treatment with control or **147** and then treated with 2mg/kg of TM for designated periods of time (n=3). **d,** Triglyceride levels in liver extracts from WT or ATF6 KO mice 24-hours post-treatment with control or **147** and then treated with 2mg/kg of TM for 12-hours (n=3). **e,** Experimental design for testing the effects of **147** in the hearts of mice subjected to 30 min of myocardial infarction, then examined 24h after the initiation of reperfusion. Red bars depict the bolus administration of the control compound, while blue bars depict the bolus administration of **147**. **f-h,** Relative infarct sizes in the heart (**f**) (n=6-7 for each trial, as shown), kidney (**g**), and brain (**h**) (n=4-5 for each trial, as shown) of male mice 24h after reperfusion. **i-k,** Plasma cTnI (**i**) (n=6-7 for each trial, as shown), plasma creatinine (j), and neurological score based on the Bederson system of behavioral patterns post-cerebral ischemic injury of male mice 24h after reperfusion of respective injury models (n=4-5 for each trial, as shown). Data are represented as mean ± s.e.m. ***P*≤0.01, ****P*≤0.001.

Supplementary FIGURE LEGENDS

Supplementary Fig. 1 –I/R activates the UPR.

a, Immunoblots of neonatal rat ventricular myocytes (NRVM) for the proteins shown after I/R or tunicamycin (TM). **b-d,** Quantification of immunoblots from NRVM subjected to normoxia or I/R. ATF6, IRE1, and PERK activation are displayed as ratios of active fragment ATF6 (50kd), spliced-XBP1 and phospho-PERK relative to ATF6 (90kd), IRE1, and PERK, respectively (n=3). **e,** Immunocytofluorescence (ICF) for GRP78 or CAT (green), alpha-actinin (red) and nuclei (TOPRO-3) in isolated adult cardiomyocytes (AMVM) post-I/R. **f, g,** Quantification of immunoblots for *Grp78* (**f**) or *Cat* (**g**) from NRVM subjected to normoxia or I/R. Data are represented as mean ± s.e.m. **P*≤0.05, ****P*≤0.001.

Supplementary Fig. 2 –Endogenous ATF6 is cardioprotective in a model of a chronic AMI.

a, qPCR for atf6 in isolated adult mouse ventricular myocytes (AMVM), isolated cardiac fibroblasts, or liver extracts from WT (n=3) or ATF6 cKO (n=3) mice. **b,** Immunoblot for Atf6 and loading control, β-actin, and IHC staining for ATF6 (cyan), tropomyosin (red), and nuclei (TOPRO-3) in LV of WT or ATF6 cKO mice. **c, d,** qPCR for IRE1 downstream target, *Erdj4*, or PERK downstream target, *Atf4* in the border zone of WT (**c**) (n=6) or ATF6 cKO (n=6) (**d**) hearts 24-hours after I/R. **e,** Malondialdehyde (MDA) in WT (n=3) and ATF6 cKO (n=3) mice 24-hours post-I/R. **f-j,** Parameters from mice 7-days post I/R. **f,** Fractional shortening. Detailed analyses of echocardiography parameters are in Extended Data Table 1 (n=5). **g,** Ratio of heart weight to body weight. **h,** Plasma cTnI. **i, j,** qPCR for *Grp78* (**i**) or *Cat* (**j**) in border zone of mice (n=3). **k,** qPCR for *Atf6* and ATF6 target genes *Grp78*, *Grp94*, and *Cat* in WT (n=3) and ATF6 cKO (n=3) mice

either 1-day or 7-days after I/R. Data are represented as mean ± s.e.m. *P≤0.05, **P≤0.01, ***P≤0.001.

Supplementary Fig. 3 –147 is selectively activates ATF6.

a, Immunoblots of UPR target proteins from NRVM 24-hours after treatment with compound **147** or tunicamycin (TM). **b-f,** Quantification of immunoblots of NRVM treated with control or **147** (n=3). **g,** Immunoblot of NRVM infected with AdV encoding Flag-ATF6 (1-670) 24-hours after treatment with control or compound **147**. Samples were performed in coordination with ChIP in Fig. 2e. **h,** Immunoblots of UPR target proteins from LV of WT (n=6) or ATF6 cKO (n=6) hearts 24-hours after treatment with control or 147. **i, j,** qPCR for *Erdj4* or *Atf4* in LV of WT (**i**) or ATF6 cKO **(j)** hearts 24-hours after treatment with control or 147. Data are represented as mean ± s.e.m. *P≤0.05, **P≤0.01, ***P≤0.001.

Supplementary Fig. 4 –147 exhibits no deleterious effects, *in vivo*.

a-c, qPCR for *Erdj4* (**a**), *Atf4* (**b**), and *Atp2a2* (**c**) following experimental design in Fig. 4a **d,** Ratio of heart weight to body weight (n=5). **e,** Plasma cTnI (n=5). **f,** Triglyceride levels in liver extracts from mice following experimental design in Fig. 4a (n=5). **g,** Plasma creatinine from mice following experimental design in Fig. 4a (n=5). **h**, qPCR for cardiac pathology genes: *Nppa* (black), *Nppb* (red), *Col1a2* (blue), and *Myh7* (green) following experimental design in Fig. 4a (n=3). **i,** qPCR for *Atf6* and ATF6 target genes *Grp78*, *Grp94*, and *Cat* in WT (n=5) mice either 8-hours, 1-day, or 7-days after a single bolus venous injection of **147** (2 mg/kg). Data are represented as mean ± s.e.m. ***P≤0.001.

Supplementary Fig. 5 –147 decreases pathological remodeling 7d post-AMI.

a-b, qPCR for *Erdj4* (**a**) or *Atf4* (**b**) in border zone of mice from Trials 4-7 of the chronic I/R protocol shown in Fig. 5a (n=3). **c,** IHC staining for GRP78 or CAT (cyan), tropomyosin (red), and nuclei (TOPRO-3) in left ventricular free wall of sham hearts or the border zone of hearts from respective trials of experimental design in Fig. 5a. Tissue sections are representative images from one mouse per condition. **d,** qPCR for cardiac pathology genes: *Nppa* (black), *Nppb* (red), *Col1a2* (blue), and *Myh7* (green) in border zone of mice from Trials 4-7 of the chronic I/R protocol shown in Fig. 5a (n=3). Statistics represent significance of entire gene sets for each trial from that of separate trials. **e,** IHC staining for cleaved caspase-3 (cyan), tropomyosin (red), and nuclei (TOPRO-3) in LV free wall of sham hearts or the border zone of hearts from indicated trials of experimental design in Fig. 5a. Tissue sections are representative images from one mouse per condition. Data are represented as mean ± s.e.m. *P≤0.05, **P≤0.01.

Supplementary Fig. 6 –147 is protective in multiple models of myocardial damage.

a, Representative images of TTC-stained post-I/R hearts from Trials 8-10 of the acute I/R protocol shown in Fig. 6e. **b, c,** Relative infarct sizes (**b**) and plasma cTnI (**c**) of female mice 24-hours after reperfusion when following the acute I/R protocol shown in Fig. 6e (n=3-4 for each trial, as shown). **d, e,** Relative infarct sizes (**d**) and plasma cTnI (**e**) of ATF6 cKO mice 24-hours post-I/R when following experimental Trials 8 (Con) and 9 (147) of the acute I/R protocol (n=4). **f,** Experimental design for testing the effects of **147** in a different model of a AMI using isoproterenol. **g-h,** Relative infarct sizes (**g**), and plasma cTnI (**h**) (n=4-5 for each trial, as shown). Data are represented as mean ± s.e.m. **P*≤0.05, ***P*≤0.01, ****P*≤0.001.

Methods

Laboratory animals. The research reported in this article has been reviewed and approved by the San Diego State University Institutional Animal Care and Use Committee (IACUC), and conforms to the Guide for the Care and Use of Laboratory Animals published by the National Research Council. ATF6-floxed mice were a generous gift from Gokhan S. Hotamisligil. Briefly, ATF6-floxed mice were generated with a targeting construct flanking exons 8 and 9 of ATF6 with LoxP sequences on a C57B/6J background, as previously described[32]. For preclinical efficacy testing of experimental compounds, wild-type (WT) 10-week old male or female C57B/6J mice were used (The Jackson Laboratory; Bar Harbor, ME). For some experiments we determined the numbers of animals to use based on a predictive power analysis to achieve 5% error and 80% power, or using the resource equation method[33]. In other experiments, the numbers of animals to use were determined practically, based on previous experiments designed to determine, for example, surgery mortality rates and the approximate magnitude of changes in the measured parameters. This was the case in experiments using ATF6 cKO mice. Our previous experiments showed that the variation in infarct size between littermates post-in vivo I/R surgeries was low, amounting to $\leq$ 5%[10]. All animal work was performed at the same time of the circadian rhythm typical of animals housed on a 12-hour light-dark cycle with ad libitum feeding. All studies in which compound 147 was administered to mice were conducted such that the surgeon and data analyst were blinded to the group assignments. Prior to all experiments, animals were assigned codes by one investigator, while investigator #2 was blinded to animal codes and nature of the treatments, e.g. control vs compound 147, performed the surgeries and echocardiographic analysis. Investigator #3 analyzed the areas at risk and infarct regions for all cardiac, renal, and cerebral ischemia reperfusion injury models; as with investigator #2, this investigator was also blinded to the animal codes and treatments. Animals were not decoded until after all surgical, functional and histological analyses were fully analyzed and relevant statistical assessments had been calculated for all parameters measured. For all animal experiments involving conditional knockout of ATF6, ATF6-floxed littermates were randomly assigned to receive AAV-control or AAV-Cre (1:1 ratio) to minimize mouse-to-mouse variability. Animals involved in I/R experiments involving administration of either the control compound, or compound 147, wild-type 10-week old male or female C57B/6J littermates. Consistency and, therefore, minimal variability of infarct sizes following ex vivo and in vivo I/R studies was ensured through blinded measurements of areas at risk relative to total left ventricular areas, as described above. As a result, we observe a variation in AAR/LV within experimental trial groups of $\leq$ 5%. For ex vivo I/R studies, mechanical error and variability were maintained as low as possible by minimizing the time between animal sacrifice and initiation of retroperfusion; our criteria is that this process must take less than 60 seconds. We find that this results in a relatively rapid progression to equilibration of heart function during ex vivo perfusion; our criteria

for reaching equilibration of LVDP is < 15 min after initiation or retroperfusion on the Langendorff apparatus.

Patient samples. Human heart explants were obtained from ventricular myocardium of patients with advanced ischemic heart failure. Control patient ventricular explants were obtained from non-failing donor hearts deemed unsuitable for transplantation for non-cardiac reasons. Samples were collected as previously described[34]. All study procedures were approved by the University of Pennsylvania Hospital Institutional Review Board.

Adeno-associated virus serotype 9 (AAV9). The plasmid encoding the human cardiac troponin T promoter driving Cre-recombinase was provided as a gift from Dr. Oliver Muller[35]. AAV9 preparation and injection were carried out as previously described[10,24]. Non-anesthetized 8-week old ATF6-floxed mice were injected with 100 μL of AAV9-control or AAV9-cTnT-Cre containing $1x10^{11}$ viral particles via the lateral tail vein using a 27-guage syringe and housed for 2 weeks before either sacrifice or experimental initiation.

Adenovirus. Construction of plasmid vectors encoding FLAG-tagged full length inactive ATF6 [ATF6(1-670)], TCR-α-HA, and empty vector (AdV-Con) has been previously described[10,24].

Cardiomyocyte isolation, culture and experimental design. Neonatal rat ventricular myocytes (NRVM) were isolated via enzymatic digestion, purified by Percoll density gradient centrifugation, and maintained in Dulbecco's modified Eagle's medium (DMEM)/F12 supplemented with 10% fetal bovine serum (FBS) and antibiotics (100 units/ml penicillin and 100 μg/ml streptomycin) on plastic culture plates that had been pre-treated with 5 μg/ml fibronectin, as previously described[10,24]. For all NRVM experiments, plating density was maintained at 4.5 x 10^5 cells/well on 12-well plates. Adult mouse ventricular myocytes (AMVM) were isolated from WT or ATF6 cKO mice 24 hours after IV injection of control compound (2mg/kg) or compound 147 (2mg/kg). AMVM isolation was performed by cannulating the ascending aorta, followed by retroperfusion and collagenase digestion, as previously described[10]. For all experiments, AMVM were plated at a density of 5.0 x 10^5 cells/well on 24-well plates that had been pre-treated with laminin (10 μg/ml) and incubated in maintaining medium (MEM medium, 1x insulin-transferrin-selenium, 10 mM HEPES, 1.2 mM $CaCl_2$ and 0.01% bovine serum albumin, 25 μM blebbistatin) for 16 hours before initiating experiments as previously described[10]. Sixteen hours after plating NRVM and AMVM were treated with control compound (10 μM), compound 147 (10 μM) or tunicamycin (10 μg/ml) for 24 hours in DMEM/F12 supplemented with bovine serum albumin (BSA) (1 mg/ml) for NRVM, or maintaining media for AMVM. For *in vitro* ischemia/reperfusion (I/R), ischemia was simulated by replacing all culture media with 0.5 ml of glucose-free DMEM containing 2% dialyzed FBS with either the control compound (10 μM), or compound 147 (10 μM), then incubated at 0.1% O_2

in a hypoxia chamber with an oxygen controller (ProOx P110 oxygen controller, Biospherix, Parish, NY) for 8 hours or 3 hours for NRVM or AMVM, respectively, as previously described[10]. Reperfusion was simulated by replacing culture media with DMEM/F12 supplemented with BSA (1 mg/ml) for NRVM or maintaining media for AMVM and incubating at 21% O_2 for an additional 24 hours. NRVM and AMVM reperfusion media were supplemented with control compound (10 μM), compound 147 (10 μM) throughout the duration of the reperfusion period. Viability was determined as numbers of calcein-AM-labeled NRVM or rod-shaped calcein-AM-labeled AMVM, using calcein-AM green (Thermo Fisher). Images were obtained with an IX70 fluorescence microscope (Olympus, Melville, NY). Numbers of viable, calcein-AM green-positive cells were counted using ImageJ or Image-Pro Plus software (Medium Cybernetics, Rockville, MD).

Small interfering RNA (siRNA) transfection. Transfection of siRNA into NRVM was achieved using HiPerfect Transfection Reagent (Qiagen, Valencia, CA) following the vendor's protocol. Briefly, NRVM culture medium was replaced with DMEM/F12 supplemented with 0.5% FBS without antibiotics, 120 nM siRNA, and 1.25 μl HiPerfect / 1 μl siRNA, then incubated for 16 hours, after which the culture medium was replaced with DMEM/F12 supplemented with BSA (1 mg/ml) for an additional 48 hours. The sequence of siRNA targeting rat ATF6 was 5-GCUCUCUUUGUUGUUGCUUAGUGGA-3, the sequence targeting rat catalase was 5-GGAACCCAAUAGGAGAUAAACUUAA-3 (cat# CatRSS302058, Stealth siRNA, Thermo Fisher), and the sequence targeting rat grp78 was 5-AGUGUUGGAAGAUUCUGA-3 (cat# 4390771, Stealth siRNA, Thermo Fisher) as previously described[10]. A non-targeting sequence (cat# 12935300, Thermo Fisher) was used as a control siRNA.

Immunoblot analysis. NRVM were lysed and subjected to immunoblot analysis, as previously described[10]. In brief, cultures were lysed with VC lysis buffer made from 20 mM Tris-HCl (pH 7.5), 150 mM NaCl, 0.1% SDS, 1% Triton X-100, protease inhibitor cocktail (Roche Diagnostics, Indianapolis, IN) and phosphatase inhibitor cocktail (Roche Diagnostics). Samples comprising 10 μg of protein were mixed with Laemmli sample buffer, boiled, then subjected to SDS-PAGE followed by transfer onto PVDF membranes for immunoblotting. Full-length Atf6 (p90) was detected with an antibody from SAB Signalway Antibody (1:1000, cat# 32008, College Park, MD), while active Atf6 (p50) was detected with an antibody from Proteintech (1:1000, cat# 24169-1-AP, Rosemont, IL). Other antibodies used include: anti-KDEL antibody (1:8,000, cat# ADI-SPA-827 , Enzo Life Sciences, Farmingdale, NY), which was used to detect GRP78, anti-catalase (1:1000, cat# ab16731, Abcam), anti-IRE1 (1:500, cat# sc-390960, Santa Cruz), anti-XBP1s (1:1000, cat# 619502, BioLegend, San Diego, CA), anti-phospho-PERK (1:1000, cat# 3179, Cell Signaling), anti-PERK (1:1000, cat# 3192, Cell Signaling), anti-Anp (1:4000, cat# T-4014 , Peninsula), anti-Gapdh (1:25000, cat# G109a, Fitzgerald Industries International Inc.), HA-probe F-7 (Santa Cruz, SC-7392; 1:1,000) and anti-FLAG (1:3,000, cat#F1804, Sigma-Aldrich, St. Louis, MO). The oxidation state of ATF6 in NRVM treated with 147 was analyzed by gel-shift

essentially as previously described[32]. Briefly, cells were lysed in low-stringency lysis buffer comprising 20 mM Tris-HCl (pH 7.5), 150 mM NaCl, 1% Triton X-100, protease inhibitor cocktail (Roche Diagnostics, Indianapolis, IN) and phosphatase inhibitor cocktail (Roche Diagnostics) and 20 μM 4-Acetamido-4'-Maleimidylstilbene-2,2'-Disulfonic Acid, Disodium Salt (AMS) (Thermo Fisher, cat# A485). AMS binds covalently to reduced thiols, typically on cysteine residues, and increases their molecular mass in SDS-PAGE. Thus, proteins that exhibit an upward shift when analyzed under non-reducing conditions compared to reducing are considered to have reduced thiols.

qPCR. Total RNA was extracted from left ventricular extract using the RNeasy Mini kit (Qiagen) as previously described[10]. All qPCR probes were obtained from Integrated DNA Technologies.

Immunocyto- and immunohistochemistry. NRVM and AMVM were plated on fibronectin and laminin-coated glass chamber slides, respectively as previously described[10]. In brief, cells were fixed with 4% paraformaldehyde, followed by permeabilization with 0.5% Triton-X. Adult mouse hearts were paraffin-embedded after fixation in neutral buffered 10% formalin via abdominal aorta retroperfusion as previously described[10]. The infarct border zone was imaged in hearts subjected to surgical I/R. The infarct border zone was identified as an area that stained positively for the cardiac muscle protein, tropomyosin that was adjacent to an area that did not stain for tropomysin (infarct zone) due to the absence of viable myocytes. The left ventricular free wall was imaged in sham and non-injured hearts. Primary antibodies used were anti-α-actinin (1:200, cat# A7811, Sigma-Aldrich), anti-tropomyosin (1:200, cat# T9283, Sigma-Aldrich), anti-GRP78 (C-20, 1:30, cat# SC-1051, Santa Cruz), anti-catalase (1:100, Abcam), anti-ATF6 (targeting to N-terminus of ATF6, 1:50, cat# sc-14250, Santa Cruz), and anti-cleaved caspase-3 (1:100, cat# D175, Cell Signaling). Slides were incubated with appropriate fluorophore-conjugated secondary antibodies (1:100, Jackson ImmunoResearch Laboratories, West Grove, PA) followed by nuclei counter stain Topro-3 (1:2000, Thermo Fisher). Images were obtained using laser scanning confocal microscopy on an LSM 710 confocal laser scanning microscope (Carl Zeiss, Oberkochen, Germany).

ERAD Assay. ER-associated degradation (ERAD) was determined using a C-terminal HA-tagged version of the model chronic misfolded substrate, TCR-α-HA as previously described[24].

Luciferase Secretion Assay. Secretory capacity of cardiac myocytes was determined essentially as described[36]. Briefly, NRVM were cotransfected with pcDNA plasmid as well as p-SV-β-galactosidase control vector and pCMV-GLuc plasmid (NEB, N8081S) using FuGENE6 (2 μg cDNA, 2:1, FuGENE:cDNA).

Chromatin immunoprecipitation (ChIP). ChIP assays were performed essentially as previously described[10]. Briefly, AdV-FLAG-ATF6(1-670) infected

NRVM were treated with fixing buffer (50 mM HEPES-KOH, pH 7.5, 100 mM NaCl, 1 mM EDTA, 0.5 mM EGTA, and 1% formaldehyde) for 10 min, quenched with 125 mM glycine, and scraped into ice-cold PBS. Cells were centrifuged, resuspended in lysis buffer (50 mM HEPES, pH 7.9, 140 mM NaCl, 1 mM EDTA, 10% glycerol, 0.5% NP-40, 0.25% Triton X-100, and protease inhibitor cocktail), and incubated on ice for 10 min. After centrifugation at 1,800 x g for 10 min, the pellets were washed with buffer containing 10 mM Tris, pH 8.1, 200 mM NaCl, 1 mM EDTA, and 0.5 mM EGTA, resuspended in shearing buffer (0.1% SDS, 1 mM EDTA, and 10 mM Tris, pH 8.1), and then transferred to microTUBEs (Covaris, Woburn, MA). Chromatin was sheared by sonication for 15 min using an M220 focused ultrasonicator (Covaris). Triton X-100 and NaCl were added to the final concentration of 1% Triton and 150 mM NaCl followed by centrifugation at 16,000 x g for 10 min. Immunoprecipitation was performed by incubated 140 µl of sheared chromatin with 5 µg of anti-FLAG antibody (cat# F1804, Sigma-Aldrich) and 260 µl of immunoprecipitation buffer (0.1% SDS, 1 mM EDTA, 10 mM Tris, pH 8.1, 1% Triton X-100, and 150 mM NaCl) at 4°C overnight. Protein A/G magnetic beads (5 µl, BcMag, Bioclone, San Diego, CA) were added to the mixtures and incubated at 4°C for 1.5 h. Magnetic beads were sequentially washed with low salt wash buffer (0.1% SDS, 1% Triton X-100, 2 mM EDTA, 20 mM HEPES-KOH, pH7.9, and 150 mM NaCl), high salt wash buffer with 500 mM NaCl, LiCl wash buffer (100 mM Tris-HCl, pH 7.5, 0.5 M LiCl, 1% NP-40, and 1% deoxycholate acid), and TE buffer (10 mM Tris-HCl, pH 8.0 and 0.1 mM EDTA). Immune complexes were eluted by incubating beads with proteinase K digestion buffer (20 mM HEPES, pH 7.9, 1 mM EDTA, 0.5% SDS, and 0.4 mg/ml proteinase K) at 50°C for 15 min. Formaldehyde crosslinking was reversed by incubating with 0.3 M NaCl and 0.3 mg/ml RNase A at 65°C overnight. Samples were further incubated with 550 µg/ml proteinase K at 50°C for 1h. DNA was purified using NucleoSpin Gel and PCR Clean-up Kit (Macherey-Nagel, Bethlehem, PA) and eluted by 30 µl of water. Two µl of DNA was used for qRT-PCR analysis with primers targeting rat Hspa5 (5'-GGTGGCATGAACCAACCAG-3' and 5'-GCTTATATATCCTCCCCGC-3'), rat Cat ERSE-1 (5'-CTACCCACCAATTAGTACCAAATAA-3' and 5'-AGAAGGGACAGGATTGGAAG-3'), rat Cat ERSE-2 (5'-CACATTCTAGGGACAGTGTAGATG-3' and 5'-ACCTTGATTATGGGCTGTGG-3'), rat Pdia6 ERSE (5'-CACATGAGCGAAATCCACAGA-3' and 5'-ACTAGTCGAGCCATGCTGAT-3'), rat HO-1 (5'-GGGCTACTCCCGTCTTCCTG-3' and 5'-CCTTTCCAGAACCCTCTACTCTACTC-3'), or rat Gapdh (5'-ATGCGGTTTCTAGGTTCACG-3' and 5'-ATGTTTTCTGGGGTGCAAAG-3'). Pdia6 served as a positive control for a known ATF6 target gene in cardiac myocytes while HO-1 and Gapdh served as negative controls as previously described[37]. ChIP signals obtained from the qRT-PCR were normalized to the input DNA.

***Ex vivo* ischemia/reperfusion.** Hearts from WT or ATF6 cKO mice that had previously received 2 mg/kg IV administration of control compound or compound 147 were rapidly excised and cannulated via the ascending aorta and subjected

to global I/R, as previously described[38]. Here, the hearts were subjected to 20 minutes global no-flow ischemia followed by reperfusion for 1 hour. Left ventricular developed pressure (LVDP) was measured using a pressure sensor balloon placed into the left ventricle and analyzed using Powerlab software (ADInstruments, Colorado Springs, CO).

***In vivo* myocardial ischemia/reperfusion.** Surgical myocardial I/R was performed as previously described[10]. Briefly, mice were anesthetized with 2% isoflurane and a thoracotomy was performed to isolate the heart, after which the left anterior descending coronary artery (LAD) was ligated with a 6-0 Prolene suture for 30 minutes, followed by suture removal and either 24 hours or 7 days of reperfusion. Regional ischemia was confirmed by visual inspection of the discoloration of the myocardium distal of the ligation, which is characteristic of impaired blood flow. Animals assigned as shams underwent the thoracotomy surgical procedure, but weren't subjected to LAD ligation. Animals were randomly assigned to trial groups prior to outset of the experiment by a single investigator, while the surgeon and data analyst were blinded to trial assignments. Animals designated to receive either control compound or compound 147 at the time of reperfusion received 2 mg/kg of respective compounds via IV injection 5 minutes prior to release of the ligation. Twenty-four hours after reperfusion, 1% of Evans Blue was injected apically to determine the area at risk (AAR). Hearts were harvested and 1-mm sections of the hearts were stained with 1% 2,3,5-triphenyltetrazolium chloride (TTC) to measure the infarcted area (INF) as previously described[36]. The AAR, INF and left ventricle area (LV) from digitized images of heart sections were analyzed using ImageJ software. For all infarct data presented, respective AAR was normalized to total LV area and all compared trials displayed the same AAR/LV ratios. A separate investigator analyzed the AAR, INF, and LV and was blinded to the animal trial assignments. Just prior to sacrifice, post-I/R, animals were anesthetized and 0.5 mL of arterial blood were obtained via inferior vena cava puncture as previously described[33]. Blood was placed in heparin- and EDTA-coated vacutainer (BD Vacutainer) and centrifuged at 3000 rpm for 10 minutes and plasma samples were analyzed for cardiac troponin I with a Mouse cTnI High-Sensitivity ELISA kit (Life Diagnostics, Inc.).

***In vivo* renal ischemia/reperfusion.** Surgical renal I/R was performed as previously described[39]. Briefly, mice were anesthetized with 2% isoflurane and a 3cm incision was made upon the abdominal midline and the abdominal cavity entered via an incision along the linea alba. The right kidney was visualized and separated from surrounding connective tissue. The right ureter and right renal portal system was permanently ligated and a right unilateral nephrectomy performed. Subsequently, the left kidney was visualized and separated from surrounding connective tissue. A Bulldog Clamp (Fine Science Tools, Foster City, CA) was applied temporarily ligating the left renal portal system for a period of 30 minutes. Global ischemia was confirmed by visual inspection of the discoloration of the kidney of the ligation, which is characteristic of impaired

blood flow. After that duration, the Bulldog Clamp was removed and the abdomen closed with instant tissue adhesive. Animals were randomly assigned to trial groups prior to outset of the experiment by a single investigator, while the data analyst was blinded to trial assignments. Animals designated to receive either control compound or compound 147 at the time of reperfusion received 2 mg/kg of respective compounds via IV injection 5 minutes prior to release of the ligation. Twenty-four hours after reperfusion, kidneys were harvested and 1-mm sections of the kidneys were stained with 1% TTC to measure the infarcted area (INF) as previously described[39]. Just prior to sacrifice, post-I/R, animals were anesthetized and 0.5 mL of arterial blood were obtained via inferior vena cava puncture as previously described[40]. Blood was placed in heparin- and EDTA-coated vacutainer (BD Vacutainer) and centrifuged at 3000 rpm for 10 minutes and plasma samples were analyzed for creatinine as a measure of glomerular filtration rate and renal functional output with a Creatinine Assay kit (Abcam).

***In vivo* cerebral ischemia/reperfusion.** Surgical cerebral I/R was performed as previously described[11]. Briefly, mice were anesthetized with 2% isoflurane and a 3 cm incision was made along the midline of the ventral surface of the neck along the left side of the trachea. The left external and internal carotid arteries were visualized and dissected from surrounding connective tissue without disturbing tangential nerves. An 8-0 catheter filament 10mm in length (Doccol Corporation) was be inserted into the middle cerebral artery (MCA) via the internal carotid artery. This occluded blood flow to the MCA and was left in position for a period of 30 minutes. After that duration, the catheter was removed and the neck closed with instant tissue adhesive. Animals were randomly assigned to trial groups prior to outset of the experiment by a single investigator, while the data analyst was blinded to trial assignments. Animals designated to receive either control compound or compound 147 at the time of reperfusion received 2 mg/kg of respective compounds via IV injection 5 minutes prior to release of the ligation. Twenty-four hours after reperfusion, brains were harvested and 1-mm sections of the brains were stained with 1% TTC to measure the infarcted area (INF) as previously described[41]. Just prior to sacrifice animals were assigned a behavioral score to assess the severity of neurological function and deficit as a result of the cerebral ischemia. The scoring was performed based on the Bederson Neurological Examination Grading System[42], where a grade of 0 corresponded to a normal function with no observable deficit, grade 1 to a moderate deficit with animals exhibiting forearm flexion, grade 2 to a severe deficit with decreased resistance to a lateral push when suspended by the tail and lethargy, and grade 3 to a severe deficit with extreme lethargy and circling behavior in the cage.

Hepatic triglyceride assay. Hepatic triglyceride assay was performed as previously described[43]. Briefly, livers were harvested and 10mg extracts were homogenized and analyzed for triglyceride content using the EnzyChrom Triglyceride Assay Kit (BioAssay Systems).

Transthoracic echocardiography. Transthoracic echocardiography was performed using an ultrasound imaging system (Vevo 2100 System, Fujifilm VisualSonics, Toronto, Ontario, Canada) as described[24]. Diastolic function was determined as previously described[40]. Briefly, echocardiography coupled with pulse-wave Doppler was used to visualize trans-mitral flow velocities and were recorded by imaging the mitral orifice at the point of the mitral leaflets. Waveforms were recorded and analyzed for peak early- and late-diastolic transmitral flow velocities corresponding to E and A waves, respectively.

Acute isoproterenol myocardial damage. Myocardial damage was induced by administering high-dose (200 mg/kg) isoproterenol via intraperitoneal injection in mice as previously described[40].

Malondialdehyde assay. Lipid peroxidation was determined by measuring the levels of malondialdehyde (MDA) using a TBARS assay kit (Cayman Chemical, Ann Arbor, MI) according to the manufacturer's instructions as previously described[10].

***In vivo* experimental compound administration.** Control compound and compound 147 were suspended to a final concentration of 0.2 mg/mL in 10% DMSO. Mice were weighed prior to administration of compounds and, subsequently, non-anesthetized 10-week old WT or ATF6 cKO mice were injected with ~250 µL of stock compounds via the lateral tail vein depending upon body mass to ensure accurate administration of 2 mg/kg. This dose was established in preliminary experiments with the control compound or compound 147 where it was shown to activate Atf6 *in vivo*; the prototypical UPR inducer, tunicamycin, which was also administered to mice at 2 mg/kg, as previously shown[44] was used as a control. Since compound 147 and tunicamycin have similar molecular weights, this dose of 147 is near the molar equivalent of the typical dose of tunicamycin. It is relevant to note that for compound 147, a dose of 2 mg/kg is similar to FDA-approved cardiovascular drugs, such as many angiotensin-converting enzyme (ACE) inhibitors, which are used in small-animal models at 2 mg/kg[45].

Statistics. For studies involving induction of myocardial damage, either through surgical I/R or isoproterenol administration, cohort sizes were based on a predictive power analysis to achieve 5% error and 80% power. All acute *in vivo* I/R studies in which compound 147 was administered in preclinical trial design were conducted such that the surgeon and data analyst was blinded to the group assignments. Two-group comparisons were performed using Student's two-tailed t-test, and all multiple group comparisons were performed using a one-way ANOVA with a Newman-Keuls post-hoc analysis. Data are represented as mean with all error bars indicating ± s.e.m. *$P \leq 0.05$, **$P \leq 0.01$, ***$P \leq 0.001$.

REFERENCES:

1 Hartl, F. U., Bracher, A. & Hayer-Hartl, M. Molecular chaperones in protein folding and proteostasis. *Nature* **475**, 324-332, doi:10.1038/nature10317 (2011).

2 Labbadia, J. & Morimoto, R. I. The biology of proteostasis in aging and disease. *Annu Rev Biochem* **84**, 435-464, doi:10.1146/annurev-biochem-060614-033955 (2015).

3 Das, I. *et al.* Preventing proteostasis diseases by selective inhibition of a phosphatase regulatory subunit. *Science* **348**, 239-242, doi:10.1126/science.aaa4484 (2015).

4 Roth, D. M. & Balch, W. E. Modeling general proteostasis: proteome balance in health and disease. *Curr Opin Cell Biol* **23**, 126-134, doi:10.1016/j.ceb.2010.11.001 (2011).

5 Walter, P. & Ron, D. The unfolded protein response: from stress pathway to homeostatic regulation. *Science* **334**, 1081-1086, doi:334/6059/1081 [pii] 10.1126/science.1209038 (2011).

6 Smith, M. H., Ploegh, H. L. & Weissman, J. S. Road to ruin: targeting proteins for degradation in the endoplasmic reticulum. *Science* **334**, 1086-1090, doi:10.1126/science.1209235 (2011).

7 Chiang, W. C., Hiramatsu, N., Messah, C., Kroeger, H. & Lin, J. H. Selective activation of ATF6 and PERK endoplasmic reticulum stress signaling pathways prevent mutant rhodopsin accumulation. *Invest Ophthalmol Vis Sci* **53**, 7159-7166, doi:10.1167/iovs.12-10222 (2012).

8 Cooley, C. B. *et al.* Unfolded protein response activation reduces secretion and extracellular aggregation of amyloidogenic immunoglobulin light chain. *Proc Natl Acad Sci U S A* **111**, 13046-13051, doi:10.1073/pnas.1406050111 (2014).

9 Martindale, J. J. *et al.* Endoplasmic reticulum stress gene induction and protection from ischemia/reperfusion injury in the hearts of transgenic mice with a tamoxifen-regulated form of ATF6. *Circ Res* **98**, 1186-1193, doi:10.1161/01.RES.0000220643.65941.8d (2006).

10 Jin, J. K. *et al.* ATF6 Decreases Myocardial Ischemia/Reperfusion Damage and Links ER Stress and Oxidative Stress Signaling Pathways in the Heart. *Circ Res* **120**, 862-875, doi:10.1161/CIRCRESAHA.116.310266 (2017).

11 Yu, Z. *et al.* Activation of the ATF6 branch of the unfolded protein response in neurons improves stroke outcome. *J Cereb Blood Flow Metab* **37**, 1069-1079, doi:10.1177/0271678X16650218 (2017).

12 Roth, G. A. *et al.* Global, Regional, and National Burden of Cardiovascular Diseases for 10 Causes, 1990 to 2015. *J Am Coll Cardiol* **70**, 1-25, doi:10.1016/j.jacc.2017.04.052 (2017).

13 Frangogiannis, N. G. Pathophysiology of Myocardial Infarction. *Compr Physiol* **5**, 1841-1875, doi:10.1002/cphy.c150006 (2015).

14 Hausenloy, D. J. & Yellon, D. M. The evolving story of "conditioning" to protect against acute myocardial ischaemia-reperfusion injury. *Heart* **93**, 649-651, doi:10.1136/hrt.2007.118828 (2007).
15 Bulluck, H., Yellon, D. M. & Hausenloy, D. J. Reducing myocardial infarct size: challenges and future opportunities. *Heart* **102**, 341-348, doi:10.1136/heartjnl-2015-307855 (2016).
16 Hausenloy, D. J. & Yellon, D. M. Ischaemic conditioning and reperfusion injury. *Nat Rev Cardiol* **13**, 193-209, doi:10.1038/nrcardio.2016.5 (2016).
17 Kalogeris, T., Baines, C. P., Krenz, M. & Korthuis, R. J. Ischemia/Reperfusion. *Compr Physiol* **7**, 113-170, doi:10.1002/cphy.c160006 (2016).
18 Murphy, E. & Steenbergen, C. Mechanisms underlying acute protection from cardiac ischemia-reperfusion injury. *Physiol Rev* **88**, 581-609, doi:10.1152/physrev.00024.2007 (2008).
19 Yellon, D. M. & Hausenloy, D. J. Myocardial reperfusion injury. *N Engl J Med* **357**, 1121-1135, doi:10.1056/NEJMra071667 (2007).
20 Plate, L. *et al.* Small molecule proteostasis regulators that reprogram the ER to reduce extracellular protein aggregation. *Elife* **5**, doi:10.7554/eLife.15550 (2016).
21 Wang, J., Lee, J., Liem, D. & Ping, P. HSPA5 Gene encoding Hsp70 chaperone BiP in the endoplasmic reticulum. *Gene* **618**, 14-23, doi:10.1016/j.gene.2017.03.005 (2017).
22 Kumar, M. *et al.* Animal models of myocardial infarction: Mainstay in clinical translation. *Regul Toxicol Pharmacol* **76**, 221-230, doi:10.1016/j.yrtph.2016.03.005 (2016).
23 Dixon, J. A. & Spinale, F. G. Pathophysiology of myocardial injury and remodeling: implications for molecular imaging. *J Nucl Med* **51 Suppl 1**, 102S-106S, doi:10.2967/jnumed.109.068213 (2010).
24 Doroudgar, S. *et al.* Hrd1 and ER-Associated Protein Degradation, ERAD, are Critical Elements of the Adaptive ER Stress Response in Cardiac Myocytes. *Circ Res* **117**, 536-546, doi:CIRCRESAHA.115.306993 [pii] 10.1161/CIRCRESAHA.115.306993 (2015).
25 Thuerauf, D. J. *et al.* Sarco/endoplasmic reticulum calcium ATPase-2 expression is regulated by ATF6 during the endoplasmic reticulum stress response: intracellular signaling of calcium stress in a cardiac myocyte model system. *J Biol Chem* **276**, 48309-48317, doi:10.1074/jbc.M107146200 M107146200 [pii] (2001).
26 Gwathmey, J. K., Yerevanian, A. & Hajjar, R. J. Targeting sarcoplasmic reticulum calcium ATPase by gene therapy. *Hum Gene Ther* **24**, 937-947, doi:10.1089/hum.2013.2512 (2013).
27 Baines, C. P. How and when do myocytes die during ischemia and reperfusion: the late phase. *J Cardiovasc Pharmacol Ther* **16**, 239-243, doi:10.1177/1074248411407769 (2011).
28 Hernandez-Resendiz, S. *et al.* The Role of Redox Dysregulation in the Inflammatory Response to Acute Myocardial Ischaemia-reperfusion Injury

- Adding Fuel to the Fire. *Curr Med Chem* **25**, 1275-1293, doi:10.2174/0929867324666170329100619 (2018).
29 Kroeger, H. *et al.* Induction of endoplasmic reticulum stress genes, BiP and chop, in genetic and environmental models of retinal degeneration. *Invest Ophthalmol Vis Sci* **53**, 7590-7599, doi:10.1167/iovs.12-10221 (2012).
30 Ron, D. & Walter, P. Signal integration in the endoplasmic reticulum unfolded protein response. *Nat Rev Mol Cell Biol* **8**, 519-529, doi:nrm2199 [pii] 10.1038/nrm2199 (2007).
31 Martinez, G., Duran-Aniotz, C., Cabral-Miranda, F., Vivar, J. P. & Hetz, C. Endoplasmic reticulum proteostasis impairment in aging. *Aging Cell* **16**, 615-623, doi:10.1111/acel.12599 (2017).
32 Engin, F. *et al.* Restoration of the unfolded protein response in pancreatic beta cells protects mice against type 1 diabetes. *Sci Transl Med* **5**, 211ra156, doi:10.1126/scitranslmed.3006534 (2013).
33 Charan, J. & Kantharia, N. D. How to calculate sample size in animal studies? *J Pharmacol Pharmacother* **4**, 303-306, doi:10.4103/0976-500X.119726 (2013).
34 Bedi, K. C., Jr. *et al.* Evidence for Intramyocardial Disruption of Lipid Metabolism and Increased Myocardial Ketone Utilization in Advanced Human Heart Failure. *Circulation* **133**, 706-716, doi:10.1161/CIRCULATIONAHA.115.017545 (2016).
35 Werfel, S. *et al.* Rapid and highly efficient inducible cardiac gene knockout in adult mice using AAV-mediated expression of Cre recombinase. *Cardiovasc Res* **104**, 15-23, doi:10.1093/cvr/cvu174 (2014).
36 Lynch, J. M. *et al.* A thrombospondin-dependent pathway for a protective ER stress response. *Cell* **149**, 1257-1268, doi:S0092-8674(12)00572-7 [pii] 10.1016/j.cell.2012.03.050 (2012).
37 Vekich, J. A., Belmont, P. J., Thuerauf, D. J. & Glembotski, C. C. Protein disulfide isomerase-associated 6 is an ATF6-inducible ER stress response protein that protects cardiac myocytes from ischemia/reperfusion-mediated cell death. *J Mol Cell Cardiol* **53**, 259-267, doi:S0022-2828(12)00182-4 [pii] 10.1016/j.yjmcc.2012.05.005 (2012).
38 Jin, J. K. *et al.* Localization of phosphorylated alphaB-crystallin to heart mitochondria during ischemia-reperfusion. *Am J Physiol Heart Circ Physiol* **294**, H337-344, doi:00881.2007 [pii] 10.1152/ajpheart.00881.2007 (2008).
39 Wei, Q. & Dong, Z. Mouse model of ischemic acute kidney injury: technical notes and tricks. *Am J Physiol Renal Physiol* **303**, F1487-1494, doi:10.1152/ajprenal.00352.2012 (2012).
40 Wallner, M. *et al.* Acute Catecholamine Exposure Causes Reversible Myocyte Injury Without Cardiac Regeneration. *Circ Res* **119**, 865-879, doi:10.1161/CIRCRESAHA.116.308687 (2016).
41 Xie, M. *et al.* Histone deacetylase inhibition blunts ischemia/reperfusion injury by inducing cardiomyocyte autophagy. *Circulation* **129**, 1139-1151, doi:10.1161/CIRCULATIONAHA.113.002416 (2014).

42 Bederson, J. B. *et al.* Rat middle cerebral artery occlusion: evaluation of the model and development of a neurologic examination. *Stroke* **17**, 472-476 (1986).
43 DeZwaan-McCabe, D. *et al.* ER Stress Inhibits Liver Fatty Acid Oxidation while Unmitigated Stress Leads to Anorexia-Induced Lipolysis and Both Liver and Kidney Steatosis. *Cell Rep* **19**, 1794-1806, doi:10.1016/j.celrep.2017.05.020 (2017).
44 Wu, J. *et al.* ATF6alpha optimizes long-term endoplasmic reticulum function to protect cells from chronic stress. *Dev Cell* **13**, 351-364, doi:S1534-5807(07)00266-3 [pii] 10.1016/j.devcel.2007.07.005 (2007).
45 Eckman, E. A. *et al.* Regulation of steady-state beta-amyloid levels in the brain by neprilysin and endothelin-converting enzyme but not angiotensin-converting enzyme. *J Biol Chem* **281**, 30471-30478, doi:10.1074/jbc.M605827200 (2006).

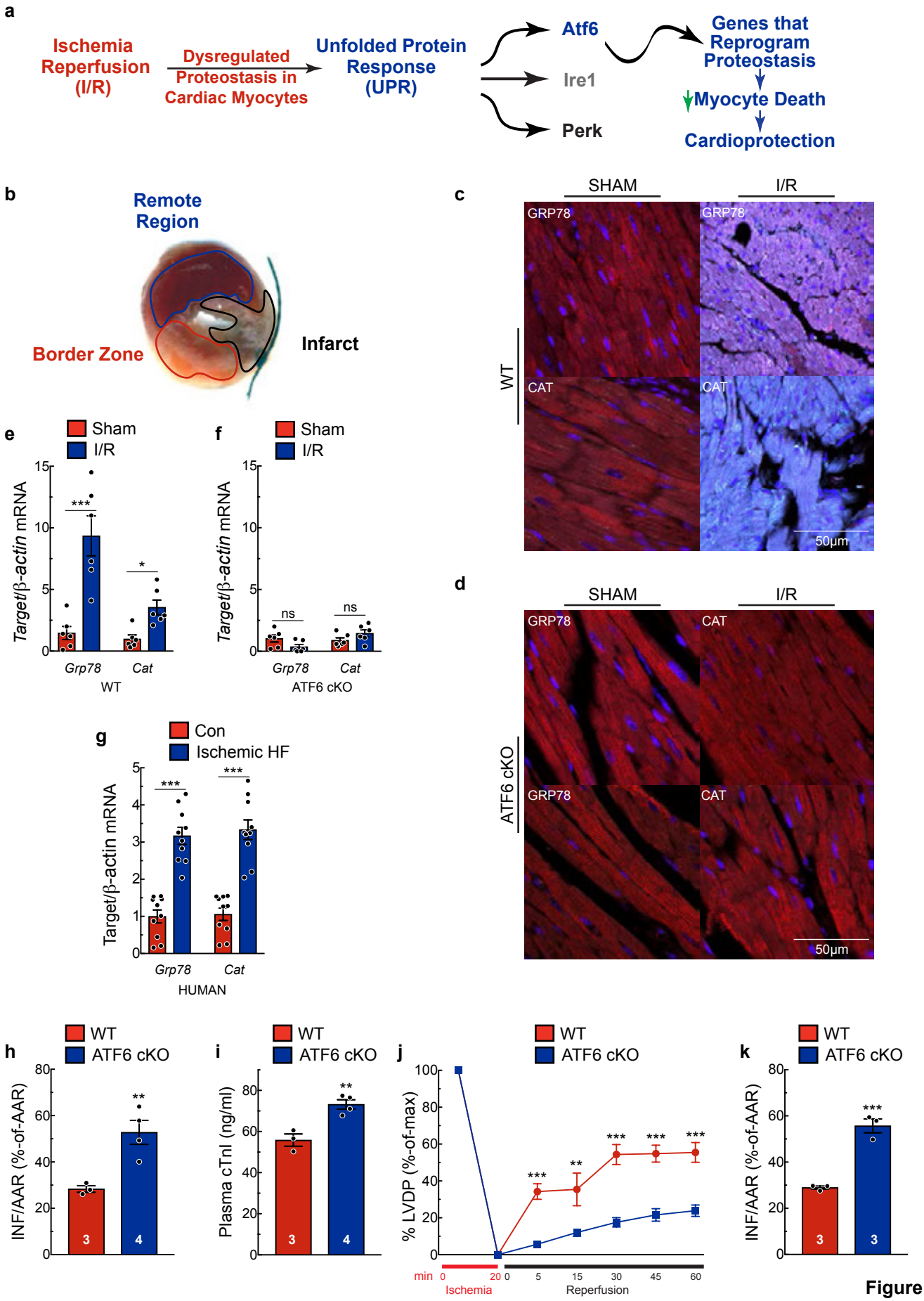
a
Ischemia Reperfusion (I/R)
Dysregulated Proteostasis in Cardiac Myocytes
Unfolded Protein Response (UPR)
Atf6
Ire1
Perk
Genes that Reprogram Proteostasis
Myocyte Death
Cardioprotection
b
Remote Region
Border Zone
Infarct
c
SHAM
I/R
WT
GRP78
CAT
50μm
d
ATF6 cKO
e
Sham
I/R
Target/β-actin mRNA
Grp78
Cat
WT
f
ATF6 cKO
ns
g
Con
Ischemic HF
HUMAN
h
WT
ATF6 cKO
INF/AAR (%-of-AAR)
i
Plasma cTnI (ng/ml)
j
% LVDP (%-of-max)
min
Ischemia
Reperfusion
k

Figure 1

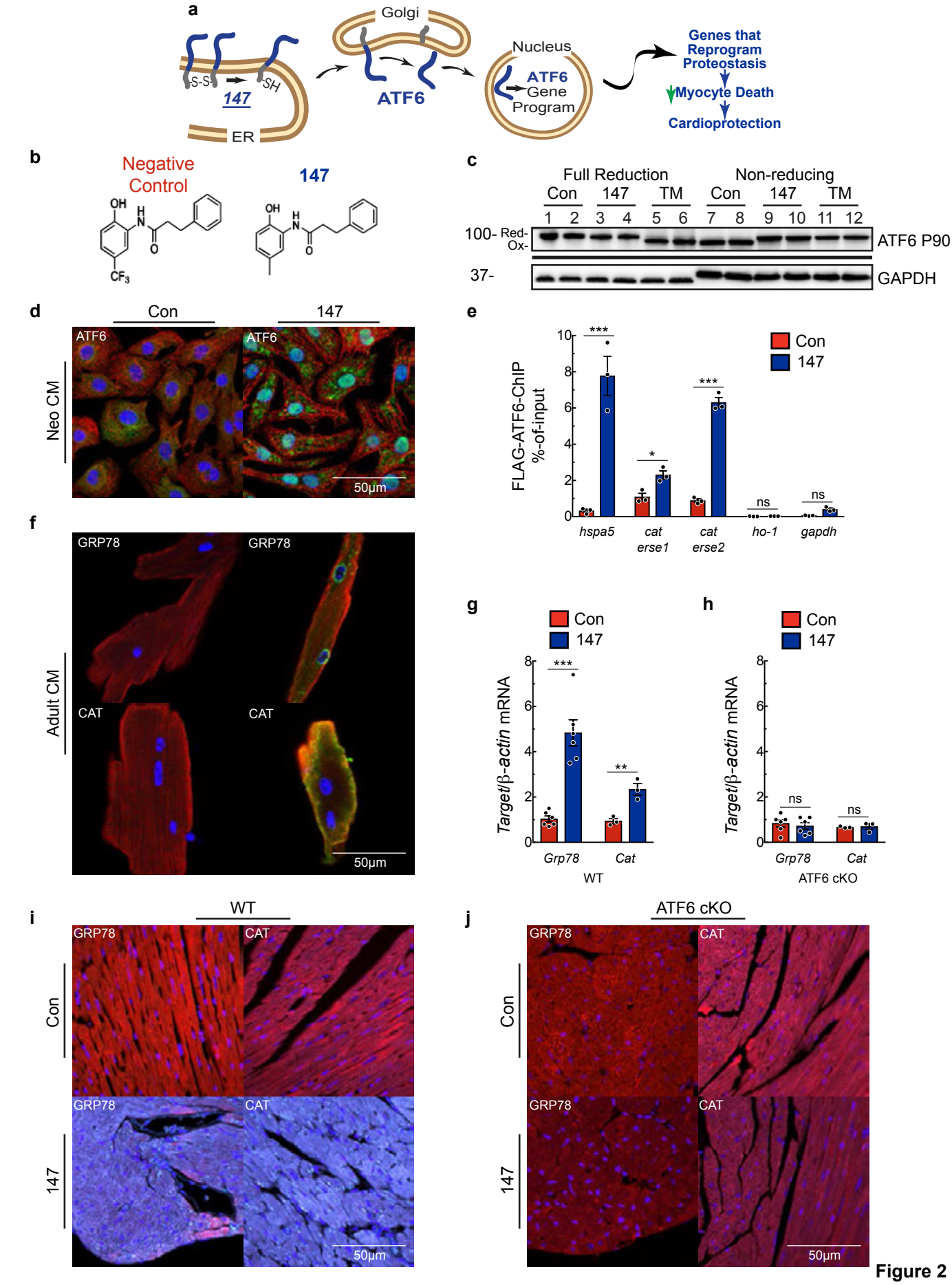
a
Golgi
S-S
SH
147
ATF6
ER
Nucleus
ATF6
Gene
Program
Genes that
Reprogram
Proteostasis
Myocyte Death
Cardioprotection
b
Negative
Control
147
OH
H
N
O
CF3
c
Full Reduction
Non-reducing
Con
147
TM
1 2 3 4 5 6 7 8 9 10 11 12
100-
Red-
Ox-
ATF6 P90
37-
GAPDH
d
Con
147
Neo CM
ATF6
50μm
e
FLAG-ATF6-ChIP
%-of-input
Con
147
***
*
ns
hspa5
cat
erse1
cat
erse2
ho-1
gapdh
f
Adult CM
GRP78
CAT
50μm
g
Target/β-actin mRNA
Grp78
Cat
WT
h
ATF6 cKO
i
WT
Con
147
GRP78
CAT
50μm
j
ATF6 cKO

Figure 2

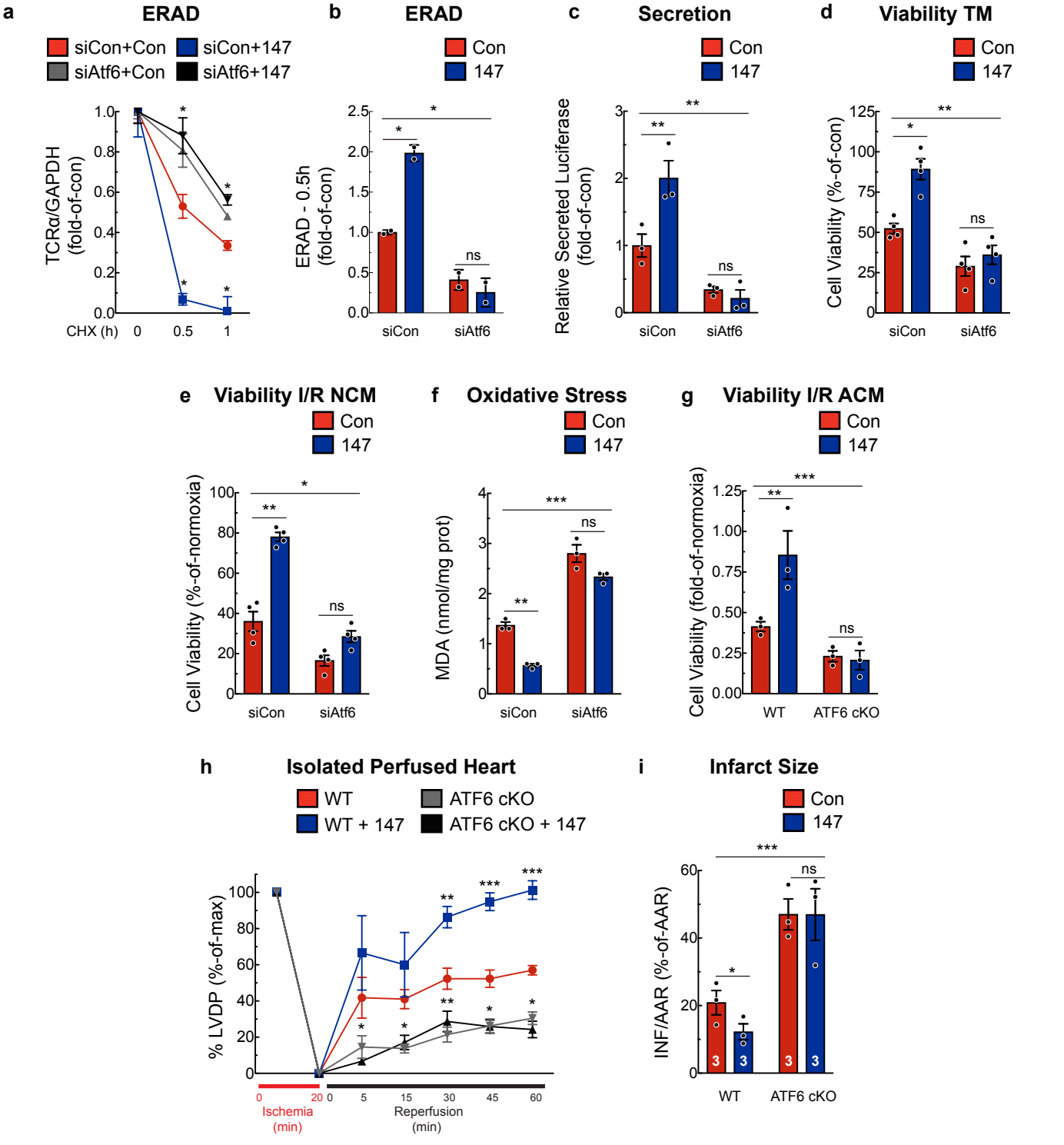
a
ERAD
siCon+Con
siCon+147
siAtf6+Con
siAtf6+147
TCRα/GAPDH (fold-of-con)
CHX (h)
b
ERAD
Con
147
ERAD - 0.5h (fold-of-con)
siCon
siAtf6
c
Secretion
Relative Secreted Luciferase (fold-of-con)
d
Viability TM
Cell Viability (%-of-con)
e
Viability I/R NCM
Cell Viability (%-of-normoxia)
f
Oxidative Stress
MDA (nmol/mg prot)
g
Viability I/R ACM
Cell Viability (fold-of-normoxia)
WT
ATF6 cKO
h
Isolated Perfused Heart
WT
WT + 147
ATF6 cKO
ATF6 cKO + 147
% LVDP (%-of-max)
Ischemia (min)
Reperfusion (min)
i
Infarct Size
INF/AAR (%-of-AAR)
ns

Figure 3

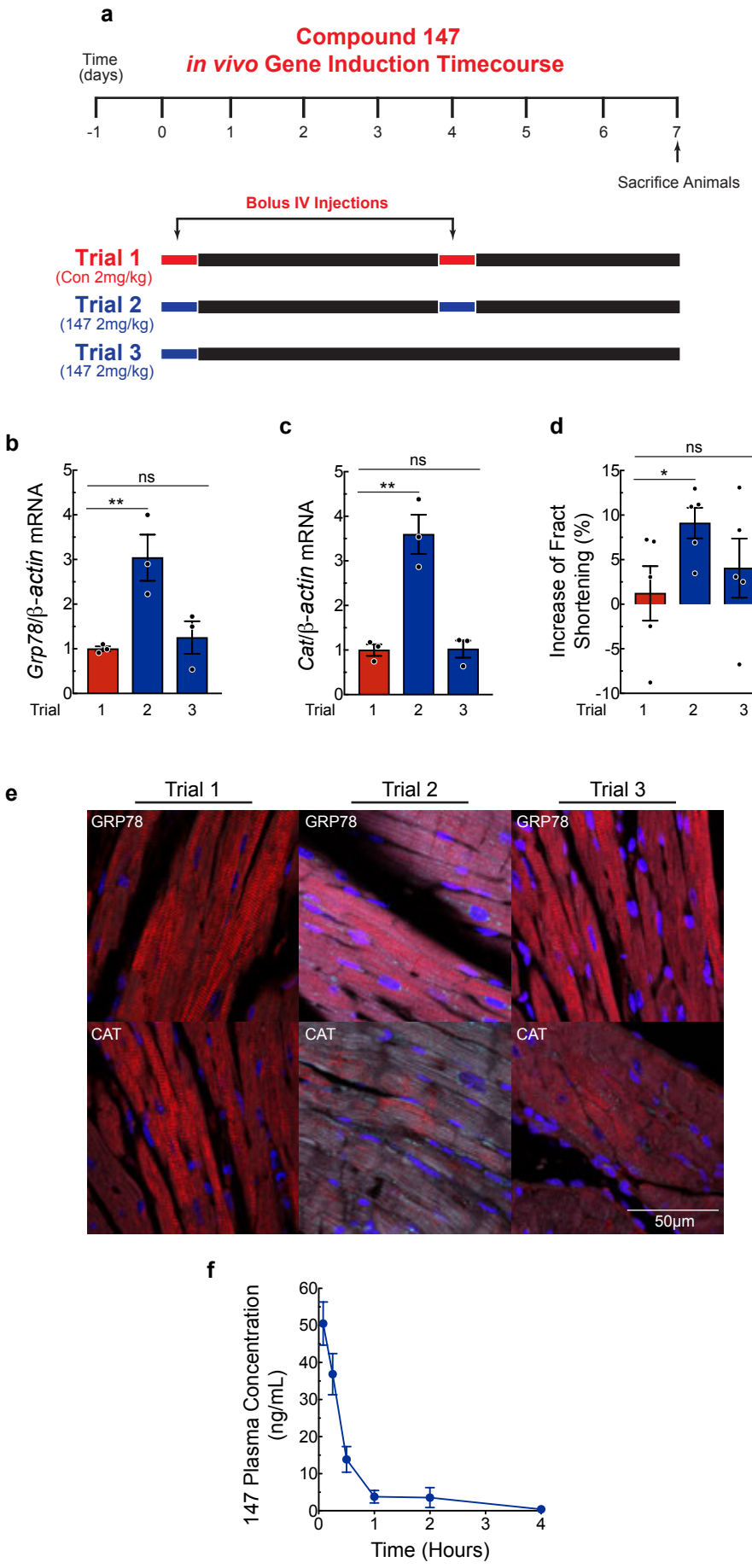
a
Compound 147
in vivo Gene Induction Timecourse
Time (days)
-1
0
1
2
3
4
5
6
7
Sacrifice Animals
Bolus IV Injections
Trial 1
(Con 2mg/kg)
Trial 2
(147 2mg/kg)
Trial 3
(147 2mg/kg)
b
Grp78/β-actin mRNA
ns
**
Trial
c
Cat/β-actin mRNA
d
Increase of Fract Shortening (%)
*
e
Trial 1
Trial 2
Trial 3
GRP78
CAT
50μm
f
147 Plasma Concentration (ng/mL)
Time (Hours)

Figure 4

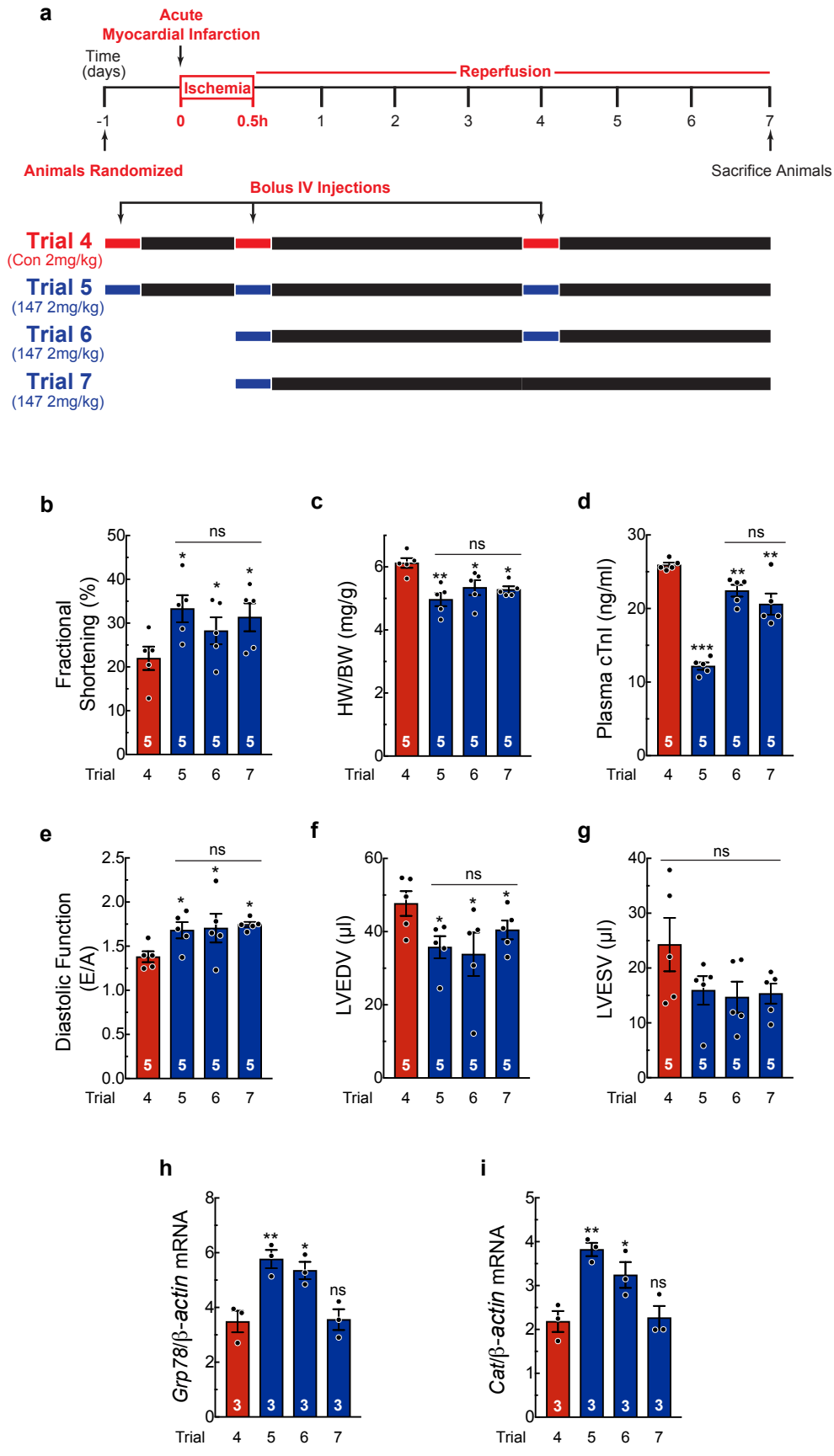
a
Acute
Myocardial Infarction
Time
(days)
Ischemia
Reperfusion
-1
0
0.5h
1
2
3
4
5
6
7
Animals Randomized
Sacrifice Animals
Bolus IV Injections
Trial 4
(Con 2mg/kg)
Trial 5
(147 2mg/kg)
Trial 6
(147 2mg/kg)
Trial 7
(147 2mg/kg)
b
Fractional Shortening (%)
c
HW/BW (mg/g)
d
Plasma cTnI (ng/ml)
e
Diastolic Function (E/A)
f
LVEDV (μl)
g
LVESV (μl)
h
Grp78/β-actin mRNA
i
Cat/β-actin mRNA
ns
Trial
4
5
6
7

Figure 5

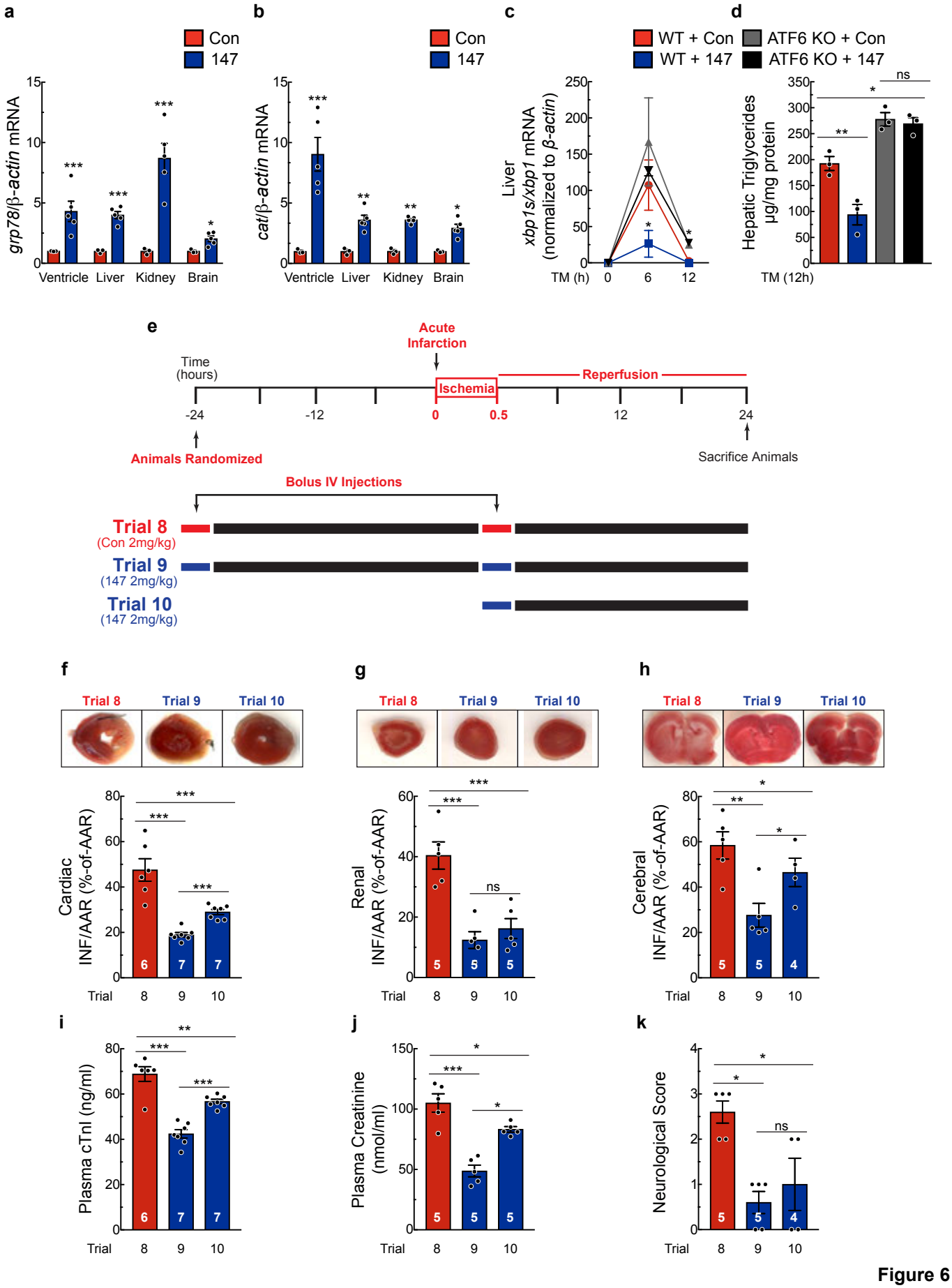
a
Con
147
grp78/β-actin mRNA
Ventricle
Liver
Kidney
Brain
b
Con
147
cat/β-actin mRNA
Ventricle
Liver
Kidney
Brain
c
WT + Con
WT + 147
ATF6 KO + Con
ATF6 KO + 147
Liver xbp1s/xbp1 mRNA (normalized to β-actin)
TM (h)
d
Hepatic Triglycerides µg/mg protein
TM (12h)
ns
e
Time (hours)
Acute Infarction
Ischemia
Reperfusion
-24
-12
0
0.5
12
24
Animals Randomized
Sacrifice Animals
Bolus IV Injections
Trial 8
(Con 2mg/kg)
Trial 9
(147 2mg/kg)
Trial 10
(147 2mg/kg)
f
Trial 8
Trial 9
Trial 10
Cardiac INF/AAR (%-of-AAR)
Trial
g
Renal INF/AAR (%-of-AAR)
ns
h
Cerebral INF/AAR (%-of-AAR)
i
Plasma cTnI (ng/ml)
j
Plasma Creatinine (nmol/ml)
k
Neurological Score
ns

Figure 6

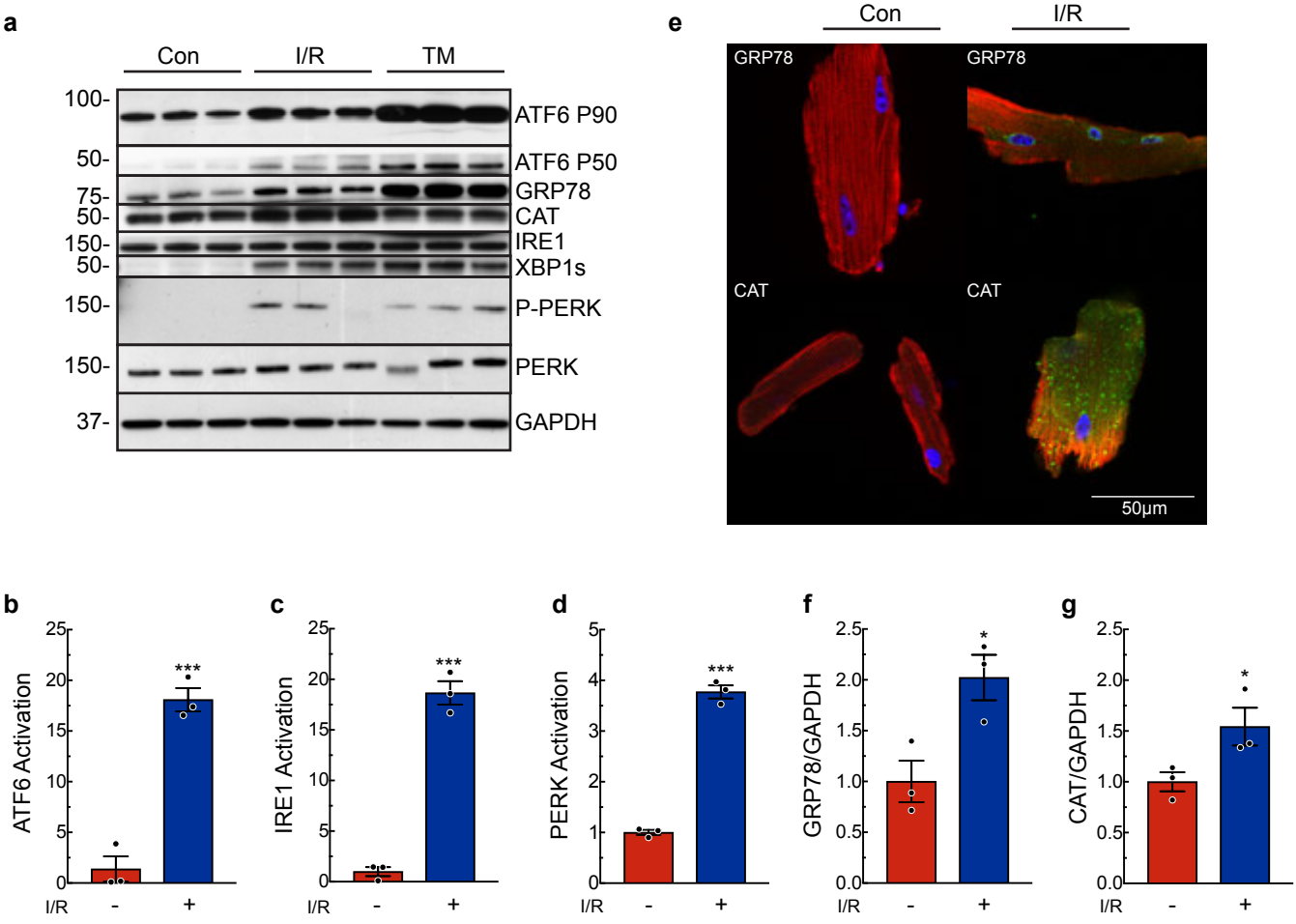

Supplementary Figure 1

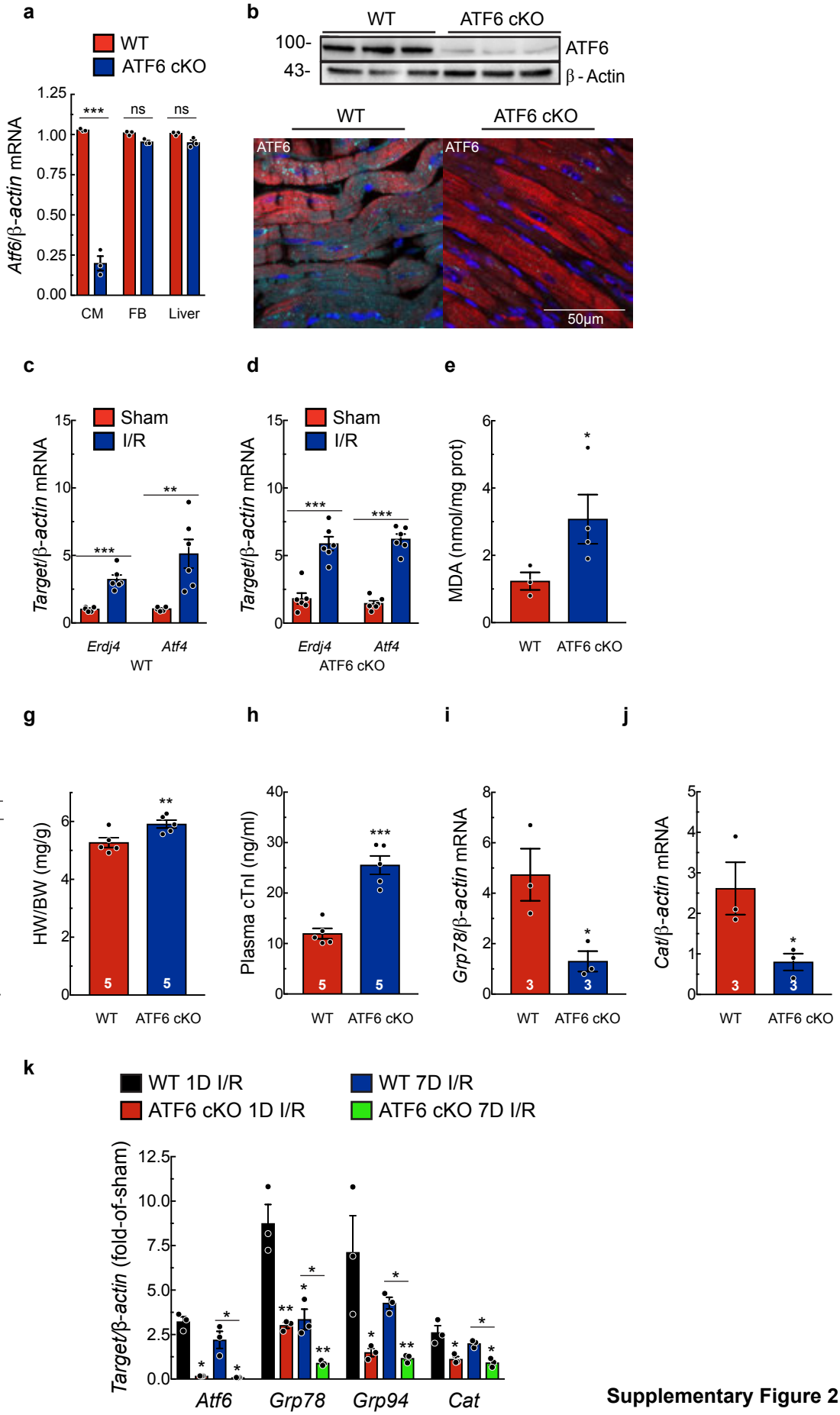

Supplementary Figure 2

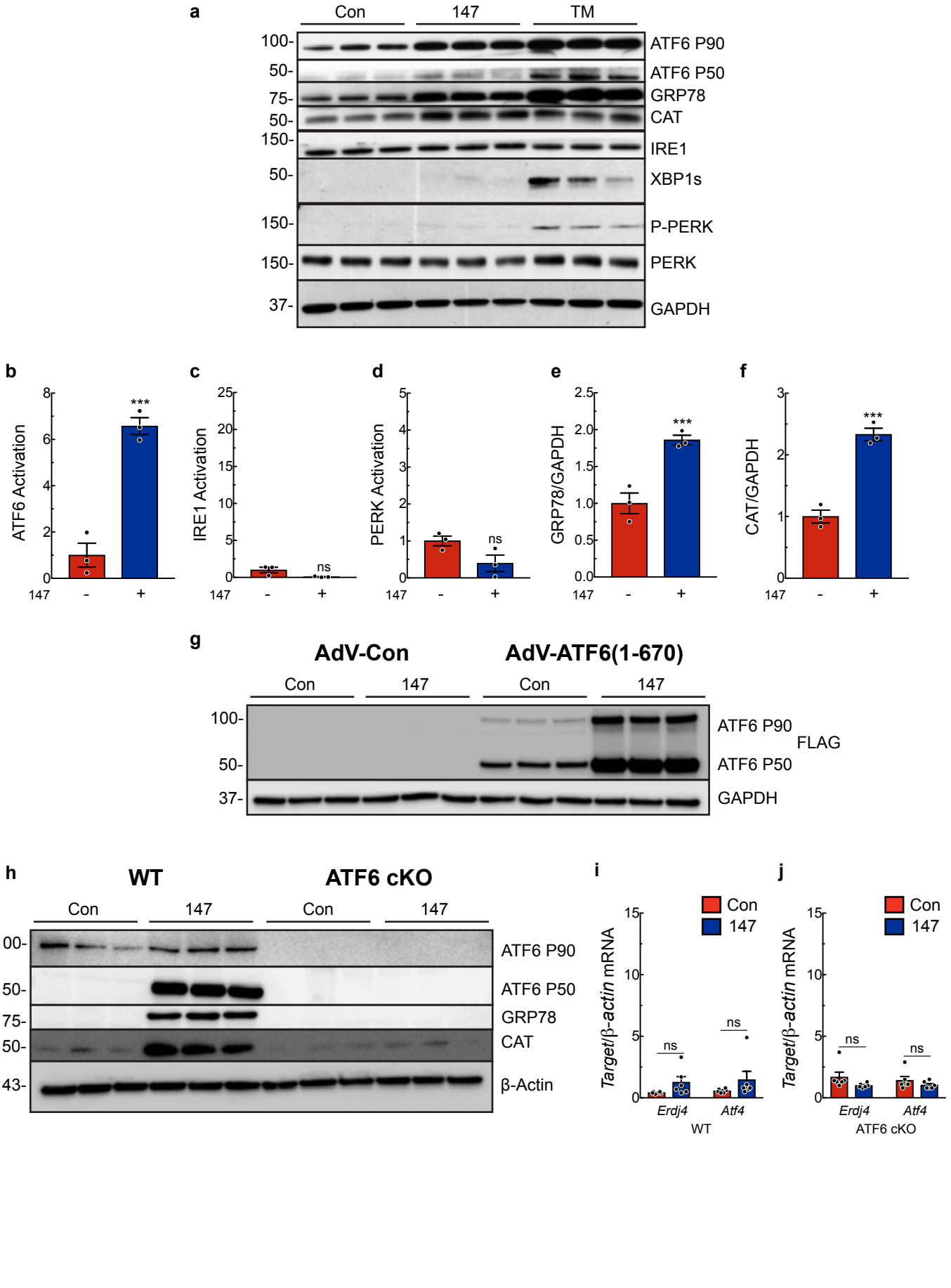

Supplementary Figure 3

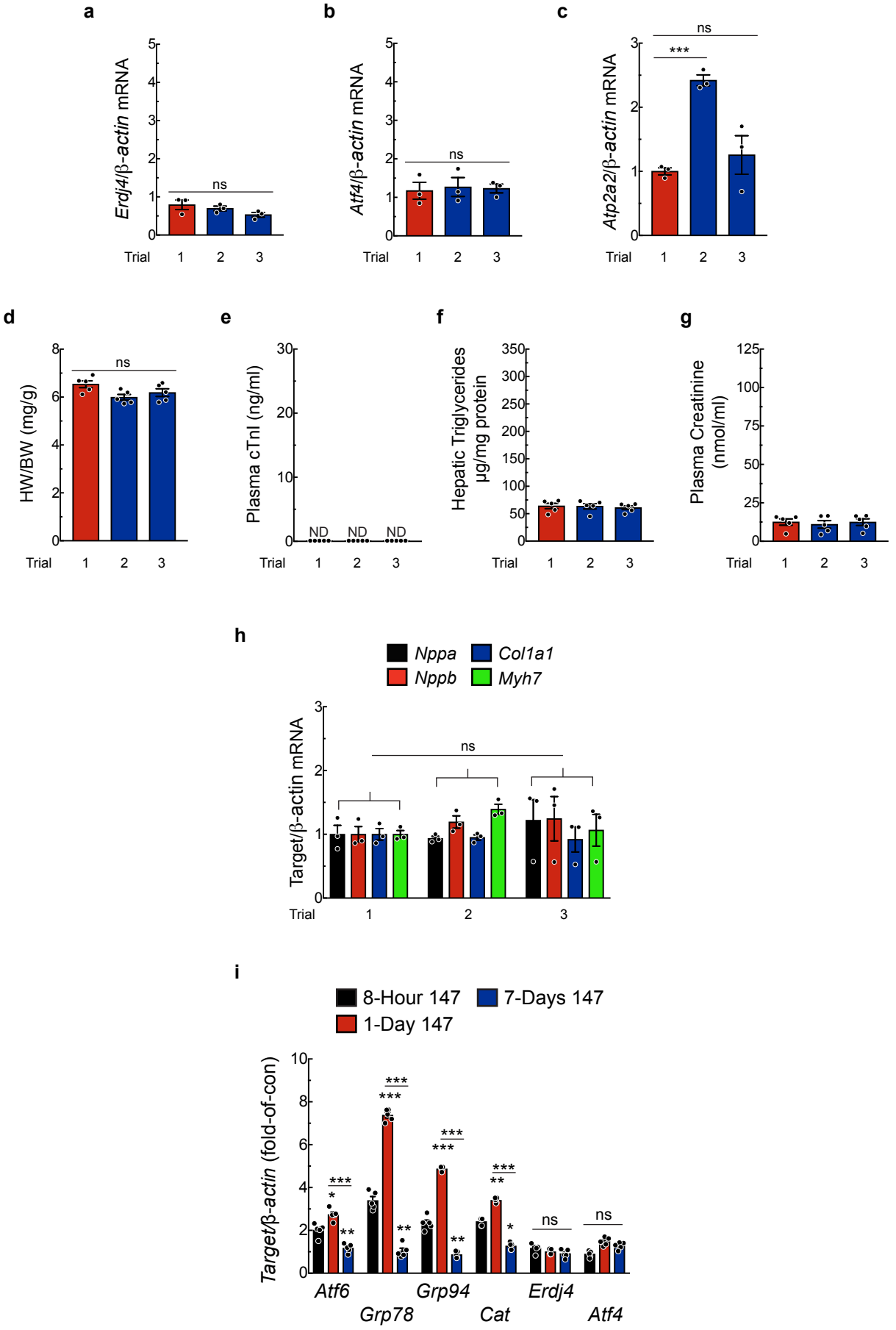

Supplementary Figure 4

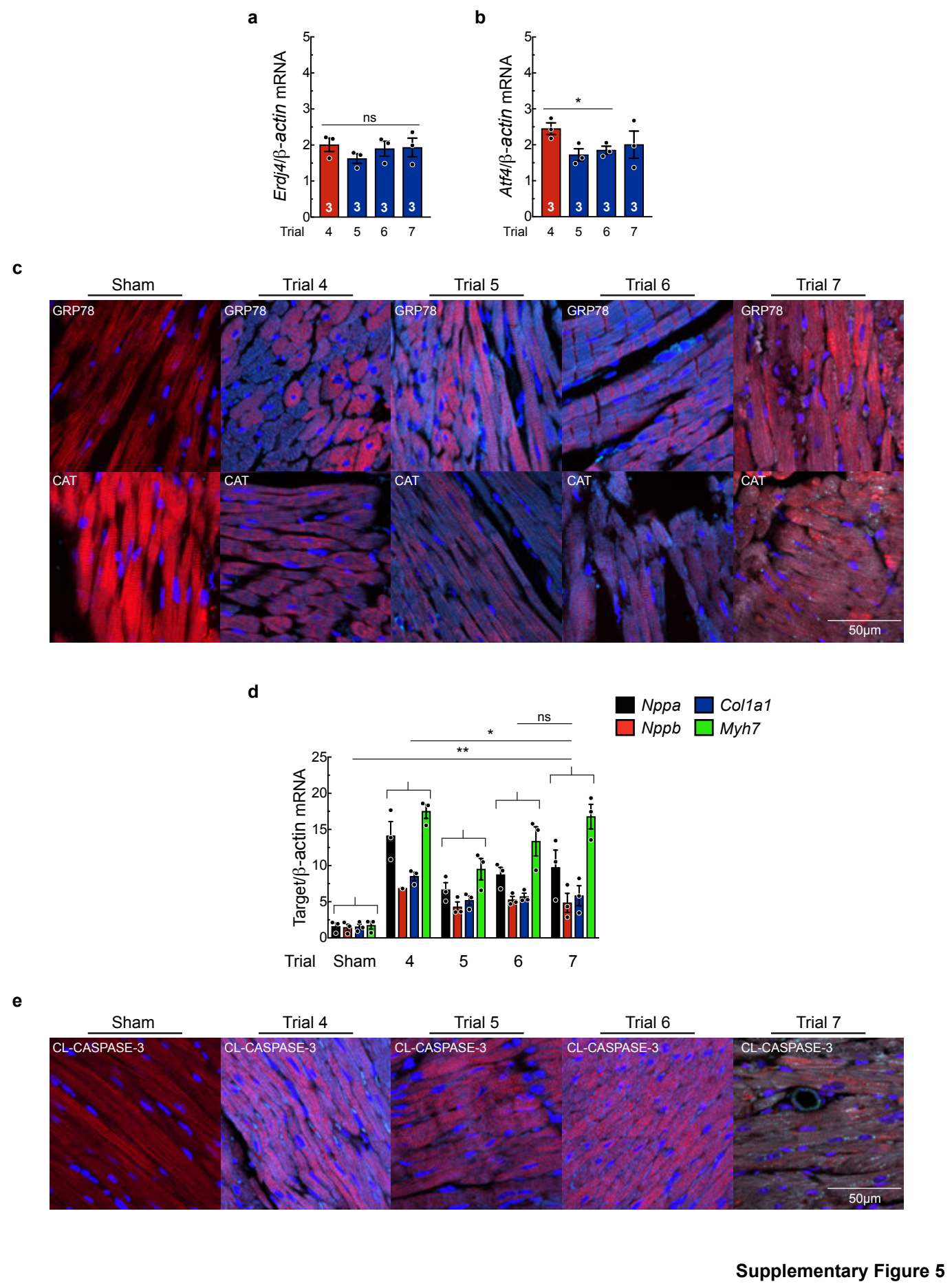

Supplementary Figure 5

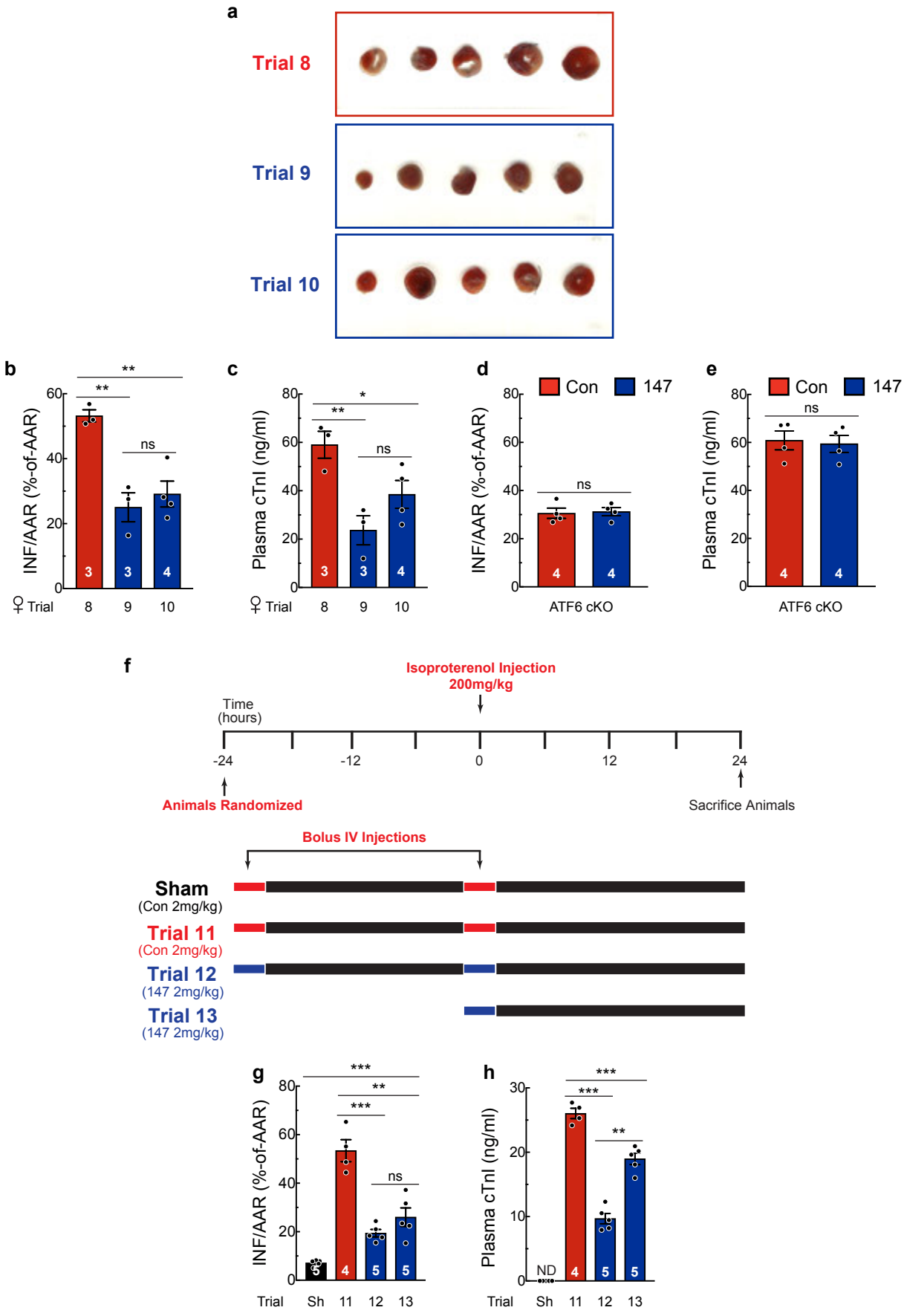

Supplementary Figure 6

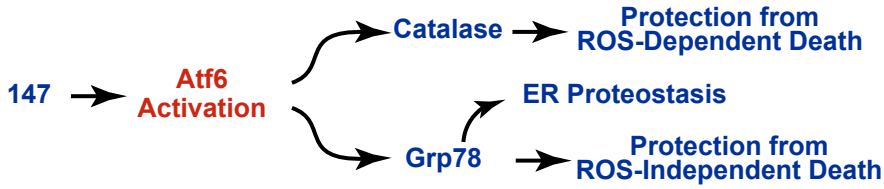

Supplementary Figure 7

Table I: 7-day I/R echocardiographic parameters

	WT Baseline (n = 5)	ATF6 cKO Baseline (n = 5)	WT Post-I/R (n = 5)	ATF6 cKO Post-I/R (n = 5)
FS (%)	34.17±1.74	36.09±1.55	25.43±1.38[1]	21.36±1.09[1,2]
EF (%)	64.37±2.38	67.22±1.88	51.07±2.52[1]	44.10±3.51[1,2]
LVEDV (μl)	41.46±2.83	36.03±3.95	43.69±4.34	55.36±4.78[1,2]
LVESV (μl)	14.86±1.62	11.59±1.06	17.61±4.42	32.22±3.51[1,2]
LVIDD (mm)	3.21±0.09	3.02±0.15	3.49±0.16[1]	3.77±0.27[1,2]
LVIDS (mm)	2.11±0.09	1.92±0.07	2.60±0.12[1]	2.83±0.27[1]
PWTD (mm)	1.47±0.13	1.43±0.10	0.97±0.15[1]	1.03±0.13[1]
PWTS (mm)	1.56±0.13	1.63±0.15	1.21±0.19[1]	1.17±0.14[1]
AWTD (mm)	0.90±0.05	0.92±0.08	0.72±0.04[1]	0.73±0.06[1]
AWTS (mm)	1.26±0.06	1.22±0.07	1.14±0.06	1.10±0.05[1]
LV mass (mg)	102.70±7.81	91.73±7.45	106.53±6.30	115.43±4.29[1,2]
HR (bpm)	504±9.96	540±9.99	543±7.54	546±6.24

FS = fractional shortening
EF = ejection fraction
LVEDV = left ventricular end diastolic volume
LVESV = left ventricular end systolic volume
LVIDD = left ventricular inner diameter in diastole
LVIDS = left ventricular inner diameter in systole
PWTD = left ventricular posterior wall thickness in diastole
PWTS = left ventricular posterior wall thickness in systole
AWTD = left ventricular anterior wall thickness in diastole
AWTS = left ventricular anterior wall thickness in systole
LV mass = left ventricular mass
HR = heart rate in beats per minute

Statistical analyses used a one-way ANOVA with a Newman-Keuls post-hoc analysis.

[1] = $p \leq 0.05$ different from respective Baseline
[2] = $p \leq 0.05$ different from WT Post-I/R

Table II: Compound 147 7-day Timecourse echocardiographic parameters

	Trial 1 Baseline (n = 5)	Trial 2 Baseline (n = 5)	Trial 3 Baseline (n = 5)	Trial 1 7-day (n = 5)	Trial 2 7-day (n = 5)	Trial 3 7-day (n = 5)
FS (%)	34.00±2.56	25.34±1.58	27.68±1.90	35.21±2.17	34.44±2.11[1]	31.73±4.11
EF (%)	64.51±3.30	51.55±2.63	55.29±3.22	66.16±2.77	65.61±2.72[1]	60.51±5.83
LVEDV (μl)	30.40±6.89	33.83±6.27	32.46±5.61	30.01±2.98	21.61±1.47[1]	32.26±3.46
LVESV (μl)	10.22±1.50	16.30±3.03	14.89±3.16	10.27±1.39	7.30±0.32[1]	13.04±2.82
LVIDD (mm)	2.78±0.23	2.91±0.22	2.87±0.20	2.81±0.11	2.46±0.07[1]	2.88±0.13
LVIDS (mm)	1.82±0.11	2.17±0.16	2.08±0.18	1.82±0.11	1.61±0.03[1]	1.98±0.17
PWTD (mm)	1.66±0.08	1.40±0.19	1.37±0.14	1.17±0.11[1]	1.80±0.03[1]	1.40±0.26
PWTS (mm)	1.76±0.05	1.67±0.17	1.45±0.10	1.43±0.12[1]	2.01±0.09[1]	1.61±0.10
AWTD (mm)	1.01±0.04	1.02±0.08	0.98±0.02	0.91±0.03	0.88±0.01	0.95±0.04
AWTS (mm)	1.22±0.13	1.19±0.05	1.20±0.06	1.29±0.04	1.16±0.07	1.21±0.11
LV mass (mg)	105.21±4.51	107.38±6.23	93.15±5.72	80.24±3.78[1]	99.78±1.89	97.21±11.04
HR (bpm)	543±9.05	493±14.51	488±40.29	522±2.76[1]	515±10.32	520±5.38

FS = fractional shortening
EF = ejection fraction
LVEDV = left ventricular end diastolic volume
LVESV = left ventricular end systolic volume
LVIDD = left ventricular inner diameter in diastole
LVIDS = left ventricular inner diameter in systole
PWTD = left ventricular posterior wall thickness in diastole
PWTS = left ventricular posterior wall thickness in systole
AWTD = left ventricular anterior wall thickness in diastole
AWTS = left ventricular anterior wall thickness in systole
LV mass = left ventricular mass
HR = heart rate in beats per minute

Statistical analyses used a one-way ANOVA with a Newman-Keuls post-hoc analysis.

[1] = $p \leq 0.05$ different from respective Baseline

Table III: Compound 147 7-day AMI echocardiographic parameters

	Trial 4 Baseline (n = 5)	Trial 5 Baseline (n = 5)	Trial 6 Baseline (n = 5)	Trial 7 Baseline (n = 5)	Trial 4 Post-AMI (n = 5)	Trial 5 Post-AMI (n = 5)	Trial 6 Post-AMI (n = 5)	Trial 7 Post-AMI (n = 5)
FS (%)	33.08±2.45	34.91±5.58	32.22±1.39	33.58±4.77	22.60±2.39[1]	33.29±3.09[2]	28.05±1.57[1,2]	31.34±3.19[2]
EF (%)	63.42±3.64	65.05±7.21	62.21±2.18	62.24±6.29	50.40±3.75[1]	62.74±4.37[2]	57.07±4.23[2]	60.03±4.74[2]
LVEDV (μl)	25.65±2.70	31.06±4.20	31.12±4.54	46.15±3.44	45.69±2.58[1]	33.81±2.33[2]	29.44±5.22[1,2]	40.46±0.561[1,2]
LVESV (μl)	9.68±1.97	11.46±3.40	12.15±2.37	18.20±3.80	21.02±3.49[1]	15.92±4.60	10.80±7.77	15.33±2.83
LVIDD (mm)	2.63±0.11	2.84±0.16	2.83±0.17	3.35±0.11	3.43±0.15[1]	3.02±0.11[2]	2.76±0.19[2]	3.18±0.08[2]
LVIDS (mm)	1.77±0.13	1.87±0.26	1.93±0.16	2.25±0.22	2.40±0.16[1]	2.15±0.17[2]	1.85±0.12[2]	2.14±0.11[2]
PWTD (mm)	1.47±0.10	1.34±0.08	1.43±0.11	0.91±0.15	1.55±0.07	1.42±0.14	1.17±0.28[1,2]	0.99±0.15[2]
PWTS (mm)	1.73±0.08	1.60±0.19	1.65±0.11	1.35±0.16	1.69±0.04	1.89±0.22	1.63±0.23	1.32±0.16
AWTD (mm)	0.88±0.02	1.02±0.08	0.88±0.03	1.01±0.04	0.87±0.04	1.04±0.09[2]	0.83±0.08	1.16±0.15
AWTS (mm)	1.12±0.05	1.31±0.09	1.17±0.05	1.28±0.06	1.17±0.04	1.43±0.12[2]	1.15±0.06	1.45±0.20
LV mass (mg)	90.82±1.26	97.68±3.33	94.12±5.52	91.03±12.18	126.30±7.43[1]	113.39±2.43[1,2]	118.22±4.96[1]	125.57±5.74[1]
HR (bpm)	522±10.54	517±20.40	545±6.88	535±11.80	507±11.32	529±9.45	492±24.50	527±7.10

FS = fractional shortening
EF = ejection fraction
LVEDV = left ventricular end diastolic volume
LVESV = left ventricular end systolic volume
LVIDD = left ventricular inner diameter in diastole
LVIDS = left ventricular inner diameter in systole
PWTD = left ventricular posterior wall thickness in diastole
PWTS = left ventricular posterior wall thickness in systole
AWTD = left ventricular anterior wall thickness in diastole
AWTS = left ventricular anterior wall thickness in systole
LV mass = left ventricular mass
HR = heart rate in beats per minute

Statistical analyses used a one-way ANOVA with a Newman-Keuls post-hoc analysis.

[1] = $p \leq 0.05$ different from respective Baseline
[2] = $p \leq 0.05$ different from Trial 4 Post-AMI

Table IV: Compound 147 24-hour AMI echocardiographic parameters

	Trial 8 Baseline (n = 3)	Trial 9 Baseline (n = 4)	Trial 10 Baseline (n = 4)	Trial 8 Post-AMI (n = 3)	Trial 9 Post-AMI (n = 4)	Trial 10 Post-AMI (n = 4)
FS (%)	35.07±1.61	33.01.91±2.75	30.94±2.75	34.06±2.41	34.70±1.13	30.27±1.86
EF (%)	66.14±2.43	63.07±4.04	60.61±4.18	64.60±3.49	65.61±1.35	58.99±2.88
LVEDV (μl)	32.00±8.38	30.74±3.75	23.34±2.70	29.22±3.21	32.17±3.63	39.03±5.67[1]
LVESV (μl)	11.32±3.68	11.70±2.38	9.40±1.93	10.73±2.34	10.92±0.81	16.46±3.14[1]
LVIDD (mm)	2.83±0.29	2.83±0.15	2.54±0.12	2.77±0.12	2.89±0.13	3.11±0.20[1]
LVIDS (mm)	1.85±0.23	1.91±0.16	1.76±0.15	1.84±0.14	1.88±0.05	2.18±0.19[1]
PWTD (mm)	1.40±0.16	1.38±0.25	1.60±0.08	1.30±0.13	1.27±0.04	1.31±0.07[1]
PWTS (mm)	1.61±0.13	1.78±0.17	1.77±0.10	1.66±0.13	1.61±0.08	1.53±0.09[1]
AWTD (mm)	1.07±0.03	0.95±0.07	0.97±0.12	1.10±0.03	0.97±0.04	0.97±0.11
AWTS (mm)	1.32±0.05	1.29±0.10	1.19±0.06	1.31±0.05	1.36±0.06	1.22±0.06
LV mass (mg)	129.50±7.91	120.70±17.09	122.45±6.31	125.02±5.62	119.03±11.24	136.04±4.34[1]
HR (bpm)	535±14.75	533±15.94	528±12.36	535±16.33	478±20.51	544±10.22

FS = fractional shortening
EF = ejection fraction
LVEDV = left ventricular end diastolic volume
LVESV = left ventricular end systolic volume
LVIDD = left ventricular inner diameter in diastole
LVIDS = left ventricular inner diameter in systole
PWTD = left ventricular posterior wall thickness in diastole
PWTS = left ventricular posterior wall thickness in systole
AWTD = left ventricular anterior wall thickness in diastole
AWTS = left ventricular anterior wall thickness in systole
LV mass = left ventricular mass
HR = heart rate in beats per minute

Statistical analyses used a one-way ANOVA with a Newman-Keuls post-hoc analysis.

[1] = $p \leq 0.05$ different from respective Baseline

Supplementary Table 4